AES/PE/09-18

Local Buckling Behaviour of a Corrosion Resistant Alloy Liner in Tight Fit Pipe due to Axial Compression

August-2009

Nabil Fathi

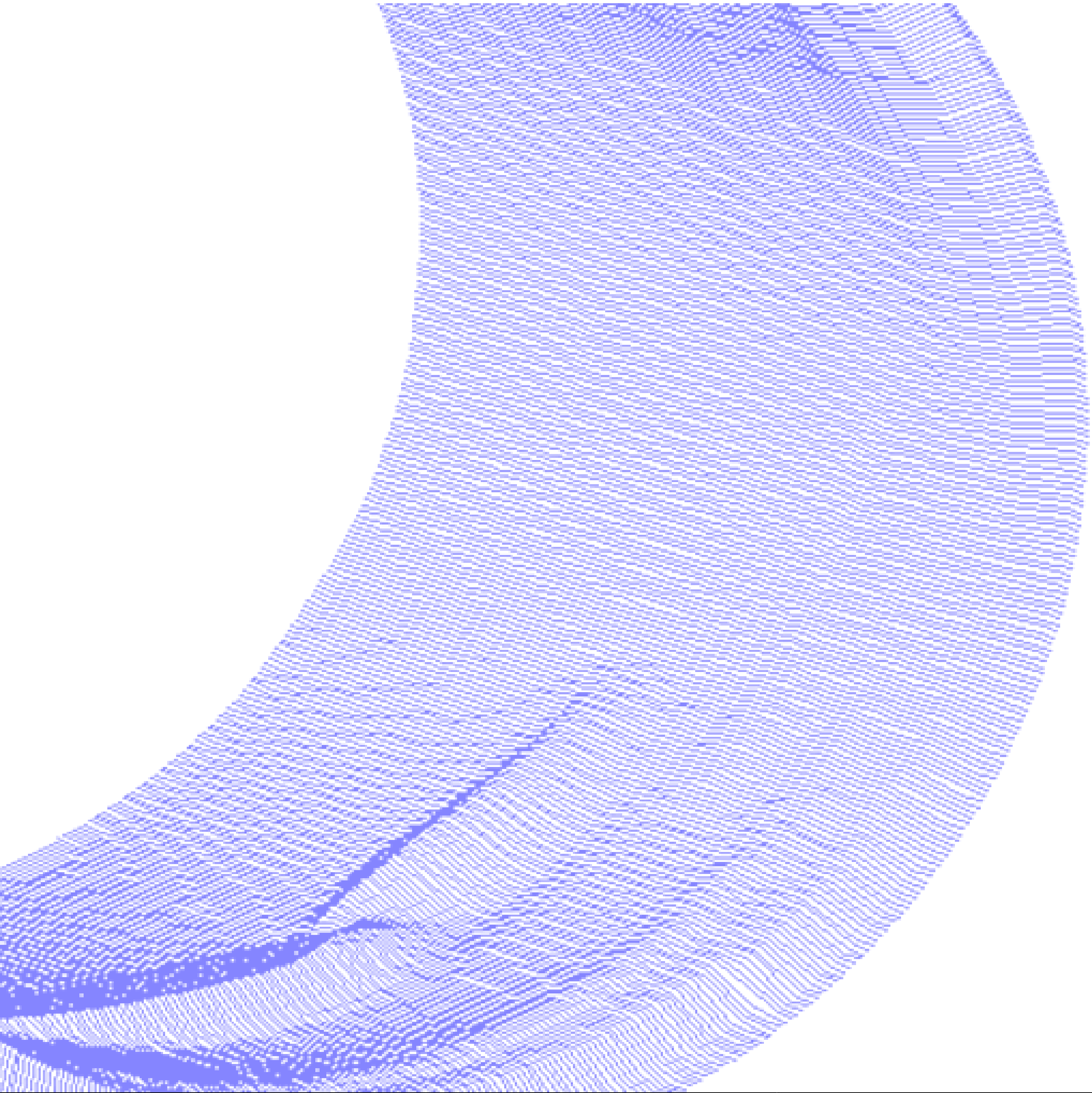

TU Delft

Department of Geotechnology

Delft University of Technology

Title	:	Local Buckling Behaviour of a Corrosion Resistant Alloy Liner in Tight Fit Pipe due to Axial Compression
Author(s)	:	Nabil Fathi
Date	:	August 2009
Professor(s)	:	Prof. dr. P.K. Currie, department of Geotechnology Prof. ir. J. Meek, Hydraulic Engineering Prof. dr. P.L.J. Zitha, department of Geotechnology Ir. A.M. Gresnigt, department of Design and Construction
TA Report number	:	AES/PE/09-18
Postal Address	:	Section for Petroleum Engineering Department of Applied Earth Sciences Delft University of Technology P.O. Box 5028 The Netherlands
Telephone	:	(31) 15 2781328 (secretary)
Telefax	:	(31) 15 2781189

Preface

This thesis has been carried out partially at the Delft University of Technology (TU Delft) and partially at HEEREMA Marine Contractors in Leiden. Eelke Focke has been my supervisor during my MSc. Thesis. This thesis has been demanding professionally and has given me the technical insight and practical experience on the used testing equipment.

First of all I would like to thank Eelke Focke who, doing her PhD. research on Tight Fit Pipe and of which this thesis is a part, helped me during the thesis period. I would also like to thank, Prof. Dr. Currie, Prof. Ir. Meek and Ir. Gresnigt, from the Delft University of Technology and Jan v. d. Graaf from HEEREMA Marine Contractors.

I want to express my appreciation to HEEREMA Marine Contractors and Jan v. d. Graaf who has been very cooperative.

In general I would like to thank the STEVIN laboratory and its employees for helping me to do my experiments.

Summary

A promising possibility to reduce corrosion resistant pipeline costs is the concept of Tight Fit Pipe, which is a double wall pipe where a Corrosion Resistant Alloy liner is mechanically fitted inside a carbon steel outer pipe. The mechanical bonding of the Tight Fit Pipe is made through a thermo-hydraulic manufacturing process.

Buckling of cylinders subjected to flexural loads (applied to Tight Fit Pipe during cost effective reeling) correlates in a number of respects to buckling of axially compressed cylinders: in both cases the critical stresses (or strains) are of the same order of magnitude and the failure modes have the same characteristics. Results from the axial compression tests provided better understanding of the buckling behaviour of Tight Fit Pipe during bending and results from this thesis study have been used as input for a bending rig construction.

The main objective of this thesis is to investigate, theoretically and experimentally, the local buckling behaviour due to axial compression of the Corrosion Resistant Alloy liner, whilst fitted in the outer pipe of the Tight Fit Pipe configuration.

The liner of the Tight Fit Pipe as tested is first analysed when not fitted in the outer pipe. The Finite Element Method used calculates the buckling stress and strain that is the most "optimistic" or upper bound, because it does not account for imperfections and local discontinuities in the material. The experimental data falls between the conservative theoretical analytical equations and the upper bound Finite Element Method data. This is as expected. The buckling shape is axi-symmetrically outward.

Secondly the liner is analysed when fitted in the outer pipe of the Tight Fit Pipe. The liner has a higher capacity in stress and strain when the liner is placed in the outer pipe, i.e. mechanically fitted, compared with the liner alone. The liner confined in the Tight Fit Pipe buckles mainly inward and buckles a-symmetrical. The buckles in the liner initiated near or on the outer pipe longitudinal weld and all buckles were not wider than 90 degrees of the total 360 degrees inner liner circumference. A more detailed analysis has been done by introducing two levels of mechanically fitted pipe, low and high induced hoop stress in the liner. High fit Tight Fit pipes had a higher maximum strain at higher maximum force, compared to low fit Tight Fit Pipes.

It can be concluded that:

a. Buckling of the liners (of TFP pipes used in the experiments), without the outer pipe, occurred outward in a single axi-symmetrical wrinkle.

b. The liners in the tight fit pipes, confined in an outer 12 ¾ inch pipes used in the experiments, buckle inward in a non-symmetrical wrinkle.

c. Wrinkles (of liners confined in an outer 12 ¾ inch pipe) do not exceed 90° of the circumference. The wrinkles have an axis which is circumferential. Wrinkles do not tend to connect with each other if more than one is present at about the same height.

d. The maximum force in the load - strain diagram was considered to be the point at which wrinkling occurred. There was a good agreement between the Finite Element results and test results for the maximum force. The FEM results for the strain at the maximum force were much higher than in the tests.

e. Buckling of a liner in a 12 ¾ inch pipe has a larger critical buckling force than a liner which is not confined in an outer pipe. This is due to the resistance to outward buckling. Bigger wrinkles must fit in a smaller radius which costs more energy than free outward buckling. This could also be the reason why the wrinkles do not tend to form as one big wrinkle in a 360 degrees radius. Outward buckling tend to occur in one axi-symmetrical wrinkle.

f. The buckling behaviour of the liner in the TFP is believed to be influenced by three different TFP properties:

1 Low or high fit (Magnitude of the residual hoop stress in the line).

2 Type of CRA material used in the liner (Material strength).

3 Type of outer pipe used, seamless or UOE-pipe (Liner to outer pipe contact irregularities)

f.1 has been proven in the test results; f.2 and f.3 are still to be proven in future work.

Recommendations for future work for improved Testing:

1 The use of real-time camera's inside the pipe is recommended for future work. Camera's, shown the buckling development with respect to time, strain and axial compression will be a excellent tool to improve understanding of buckling behaviour.

Stopping the test sequence to check the liner for buckling can be avoided. This will have effect on the whole experiment, because unloading and re-compressing the test specimens can alter the configuration and is not simple to replicate.

Recommendations for future work for an Improved FEM model:

2 The following is a recommendation for future work in modelling and comparing FEM results to experimental tests. A scan with, for example PLUTO (ID-scanner), can be made of the pipe before and after experimental testing. The scans may be used in a Finite Element (FE) program to generate a geometry with the imperfections (dents and bulges) and exact pipe dimensions (pipe ovality).

A FEM model with identical properties (e.g. material unconformities) and pipe geometry (a 3D-scan) from a test specimen will give less discrepancies between experimental and FEM results. This will give a better prediction of buckling force and strain.

For better and further advanced understanding of behaviour of buckling of the liner of the TFP:

3. Tests with different CRA materials, with different material properties

4. Tests with seamless inner liner and outer pipe to compare with pipes with a weld seam.

5. Tests with spirally welded pipes to compare with longitudinally welded pipes and seamless pipes.

6. Tests that axially compress the integrated TFP (inner liner with outer pipe)

Table of Contents

List of Symbols and Abbreviations

Latin Symbols:

E	Young's modulus or modulus of elasticity [MPa]
L	length [mm]
r	radius [mm]
t	Wall thickness [mm]

Greek Symbols:

ε	Strain [-]
η	Reduction factor [-]
μ	Gerard factor [-]
ν	Poisson's ratio [-]
π	Mathematical constant [approximately equal to 3.14159]
σ	Stress [MPa]
ω	Half-wave length [mm]

Subscripts and Superscripts:

Cr	critical
max	maximum
P	plastic
S	secant
t	tangent

Abbreviations:

CO_2	Carbon dioxide
CRA	Corrosion Resistant Alloy
D/t	Diameter over thickness
FE	Finite Element
FEM	Finite Element Method
H_2S	Hydrogen sulphide
IR	Inside Radius
LVDT	Linear Variable Displacement Transducer
OD	Outer Diameter
OR	Outside Radius
Ref.	Reference
SG	Strain Gauge
TFP	Tight Fit Pipe

1 Thesis Introduction

1.1 Background Information

Hydrocarbons being transported from a production location or from the well to a treating station may contain hydrogen sulphide (H_2S), carbon dioxide (CO_2) and other corrosive products or components that require the use of corrosion resistant alloys (CRA). These CRA's are needed for tubing in the well and in the pipeline to the treating station if no chemical corrosion inhibition is present or extra wall thickness. A promising possibility to reduce corrosion resistant pipeline costs is the concept of Tight Fit Pipe (TFP; trade name of Kuroki T&P Co. Ltd.), which is a double wall pipe where a CRA liner is mechanically fitted inside a carbon steel outer pipe. The mechanical bonding of the TFP is made through a thermo-hydraulic manufacturing process [Ref. 6].

1.2 Tight Fit Pipe Manufacturing Overview

The manufacturing process starts by positioning a hydraulic expansion machine (which is also a cooling machine) inside the liner pipe. The machine will pump cooling water through the liner such that the liner pipe will be at the temperature of the cooling water. The liner including the cooling machine is then inserted in an outer pipe which is heated in an oven. Internal overpressure is then created by the hydraulic pressure of the flowing cooling water. The liner pipe is hydraulically expanded and will yield during the pressure increase. The liner expands plastically and makes contact with the outer pipe at increase of internal pressure to maximum (OD also increases in size). The hydraulic overpressure of the cooling water is now removed, but the cooling water and oven are still active. The TFP is taken out of the oven and cooled down to room temperature. This thermo-hydraulic process is schematically depicted in Figure 1-1 and explained in Appendix A.

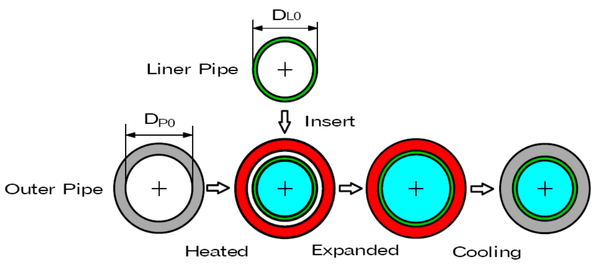

Figure 1-1 TFP thermo-hydraulic manufacturing process [Ref. 41]

1.3 Reeling Installation Method

A cost effective method of installing pipelines offshore is by means of reeling. Reeling involves welding pipe joints to form a pipe string that may have a length of several kilometres, after which the entire pipe string is wound onto a spool (Figure 1-2), which is positioned on a vessel. The reel vessel then sails to the offshore location where the pipe string is unwound and straightened. Generally reeling is a cost effective method for installing pipe due to the fact that the pipeline sections are welded together in non-critical vessel time. However, it has to be taken into account that the vessel has to sail back and forth between the reeling location (or spool base) and the offshore installation location. This distance may have to be crossed several times depending on the maximum reel size and total pipeline length to be laid. If this distance is not too large, reeling is a very effective method of pipeline installation offshore.

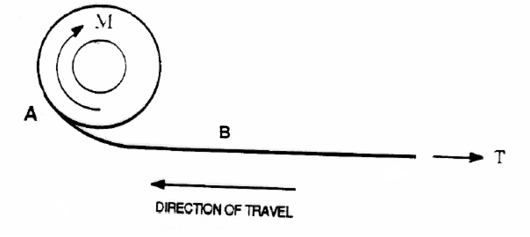

reeling on the spool

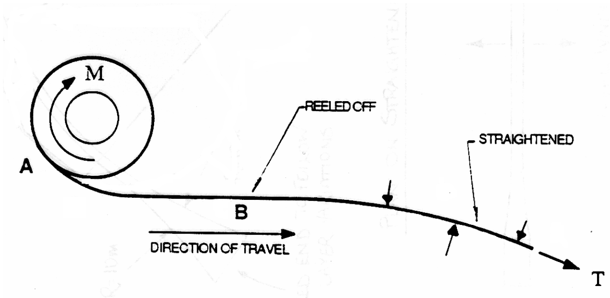

reeling off the spool

Figure 1-2 Reeling of a pipe string
Note: **A** is the spool, with **M** as moment of force applied on the spool with its direction arrow, **B** as Pipe string (pipe string direction of travel on and off the spool) and **T** as tension needed during reeling

For single walled pipeline, with an outer diameter (OD) of 4 to 18 inch, reeling is a proven technology. Reeling of TFP is however not yet a proven technology because it is still to be demonstrated for which conditions, pipe dimensions and pipe properties unacceptable wrinkling is avoided. If it is possible to install TFP by reeling it would be an attractive new option for many corrosive offshore fields.

1.4 Research

The possibility of reeling TFP is recently being investigated in a PhD research project (Ref. 13). The main objective of the overall PhD research (of which this master thesis is a part) was to investigate whether it is possible to install TFP by means of reeling. This is researched theoretically and experimentally by bending tests on TFP. The TFP is bent in a purpose-built bending rig, located at the Delft University of Technology, Department of Civil Engineering. The bending tests are needed to demonstrate the behaviour of TFP when it is subjected to the reeling process. In these bending experiments the reel size at which the liner pipe starts to wrinkle is investigated. The TFP is bent step by step on to smaller reels, while wrinkle development in the liner followed.

Buckling of cylinders subjected to flexural loads (applied to the TFP during reeling) correlates in a number of respects to buckling of axially compressed cylinders: in both cases the critical stresses (or strains) are of the same order of magnitude [Ref. 33]. Axial compression tests were therefore executed on the TFP prior to completion of building the bending rig. The axial compression machine was readily available making axial compression tests possible while a bending rig still had to be built. Results from the axial compression tests provided better understanding of the buckling behaviour of TFP and results from these axial tests were used as input for the bending rig construction.

1.5 Objective of this Master Thesis

This master thesis focuses on two different kinds of axial compression tests on the TFP:

I. Axial compression of only the liner, determining the axial buckling strength and behaviour of the liner alone.

II. Axial compression of the liner while it is confined in the outer pipe. The liner is axially compressed, while the outer pipe is not.

These two types of tests provide insight into the influence of the presence of the outer pipe on the buckling behaviour of the liner. The experimental results of the two types of experiments (tests I and II) are verified by means of analytical equations and Finite Element (FE) models. The main objective of this thesis is to investigate theoretically and experimentally, the local buckling behaviour due to axial compression of the CRA liner, while confined in the outer pipe in the Tight Fit Pipe configuration.

1.6 Structure of this Master Thesis

This thesis is divided into several parts, Chapter 1 to Chapter 5:

Chapter 1 gives an introduction of the thesis in which the TFP manufacturing process and reeling is explained.

Chapter 2 is an investigation of the axial buckling behaviour of only the liner pipe, coming from a 12 ¾-inch TFP, by means of experiments, analytical equations and Finite Element (FE models). The results will be compared in this chapter.

Chapter 3 focuses on axial compression of the liner when confined in the outer pipe of a 12 ¾-inch TFP. This will be researched by means of experiments and Finite Element models. Results will be compared.

Chapter 4 concludes this thesis and presents recommendations for future work.

2 Axial Compression of only the Liner Pipe of a 12 ¾-inch Tight Fit Pipe

2.1 Introduction

The Tight Fit Pipe (TFP) liner is the inner pipe of the TFP and is obtained by removing the outer pipe by longitudinal saw cutting a TFP specimen. The obtained liner has a smaller outer diameter (OD) then the mentioned 12 ¾-inch TFP, but the liner alone will be called the 12 ¾-inch TFP liner in this thesis, from this point forward. This liner is used in the experiments and has some specific properties.

The liner pipe is made of the corrosion resistant alloy (CRA) 316L material. The geometry and material properties of the 316L liner pipe can be found in Table 2-1;

Table 2-1: Liner geometry and material properties

	Outer diameter*	Wall thickness*	Liner length*	Modulus of Elasticity (E)*	0.2 % yield Strength*	Poisson's ratio (ν)#
[Unit]	[mm]	[mm]	[mm]	[MPa]	[MPa]	[-]
Value	296	3.0	100	193000	305	0.3

Note *: Averaged data from measurements on 316L Liner

Note #: Data used is assumed applicable on stainless steel type 316L

This liner will be used in the experiments to analyse the liner buckling behaviour. This experiment is modelled in a Finite Element (FE) program (MSC.MARC) The critical buckling strain will be predicted using analytical equations and compared to experimental results.

2.2 Experiment Configuration and Preparation

The objective of the 12 ¾-inch TFP liner experiments is to experimentally determine the buckling strain and force of the six liner specimens available for testing. These experiments are preformed with use of an apparatus which will induce an axial compression force on the liner. This apparatus consists of a hydraulically powered piston which is able to produce compressive force up to of 5000 kN (The apparatus setup is discussed into detail in Appendix B.

The axial compression apparatus configuration uses basically two plates to compress the liner and this is illustrated here below in Figure 2-1.

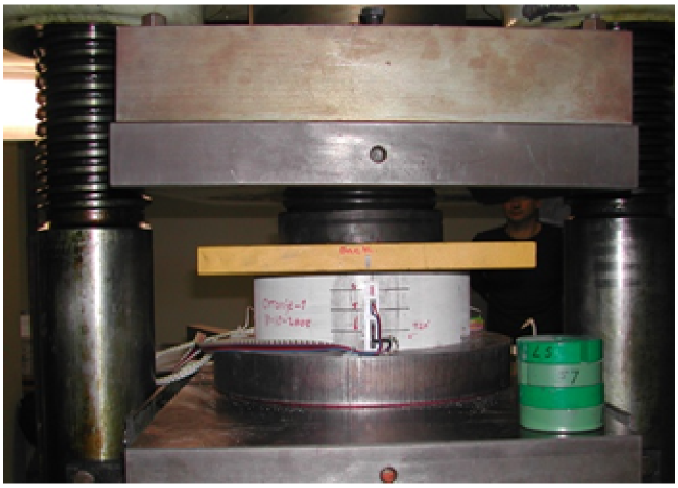

Figure 2-1: Liner specimen placed in the compression apparatus

The liner samples are machined at the outer ends to create an even compression surface. Nine axial strain gauges were attached to each liner. The strain gauges are placed from top to bottom (at ¼, ½ and ¾ of the liner height at:

- 0° degrees with strain gauge SG-1, SG-2 and SG-3
- 120° degrees with strain gauge SG-4, SG-5 and SG-6
- 240° degrees with strain gauge SG-7, SG-8 and SG-9

as can be seen in Figure 2-2.

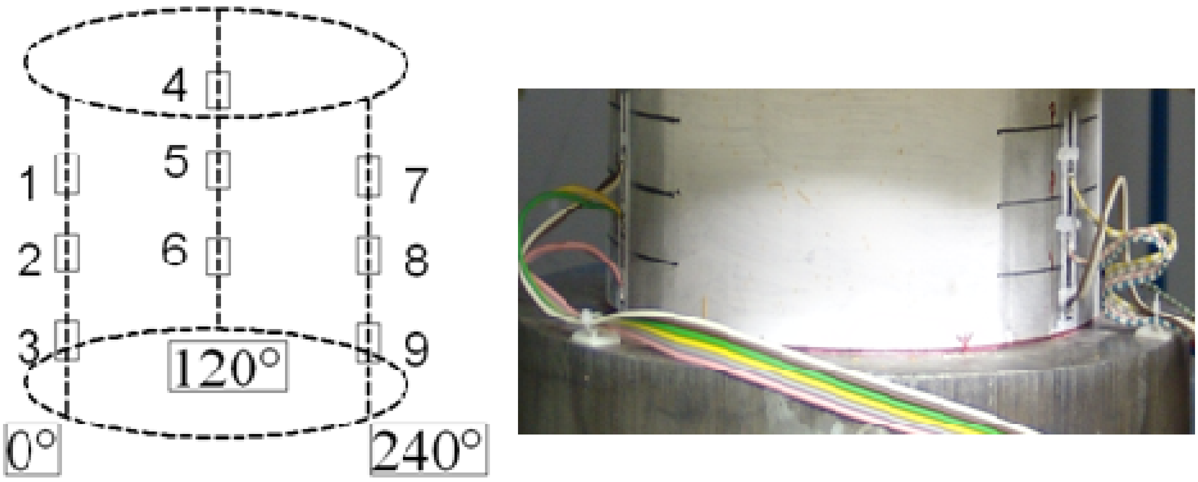

Figure 2-2: Strain gauges configuration on the liner samples

2.3 Procedure of the Axial Compression tests of the Liner

The general test procedure of the preformed experiments is explained next.

The axial compression experiments of the liner consist of stages I and II:

I. The Stage I consists of an increasing the axial force to 300 kN to remove any play or leeway in the test equipment and setup. The force remains within the elastic envelope such to cause no permanent deformation of the liner. The force is then released gradually to zero.

II. In Stage II the force is increased until liner buckling occurs. The buckling force in the axial compression tests is identified as the maximum force that could be applied onto the test specimen. The buckling strain is defined as the strain measured at the critical force.

The two stages are illustrated in an axial force strain diagram in Figure 2-3, with stage I (example data) as the open triangles and stage II (example data) as the closed circles.

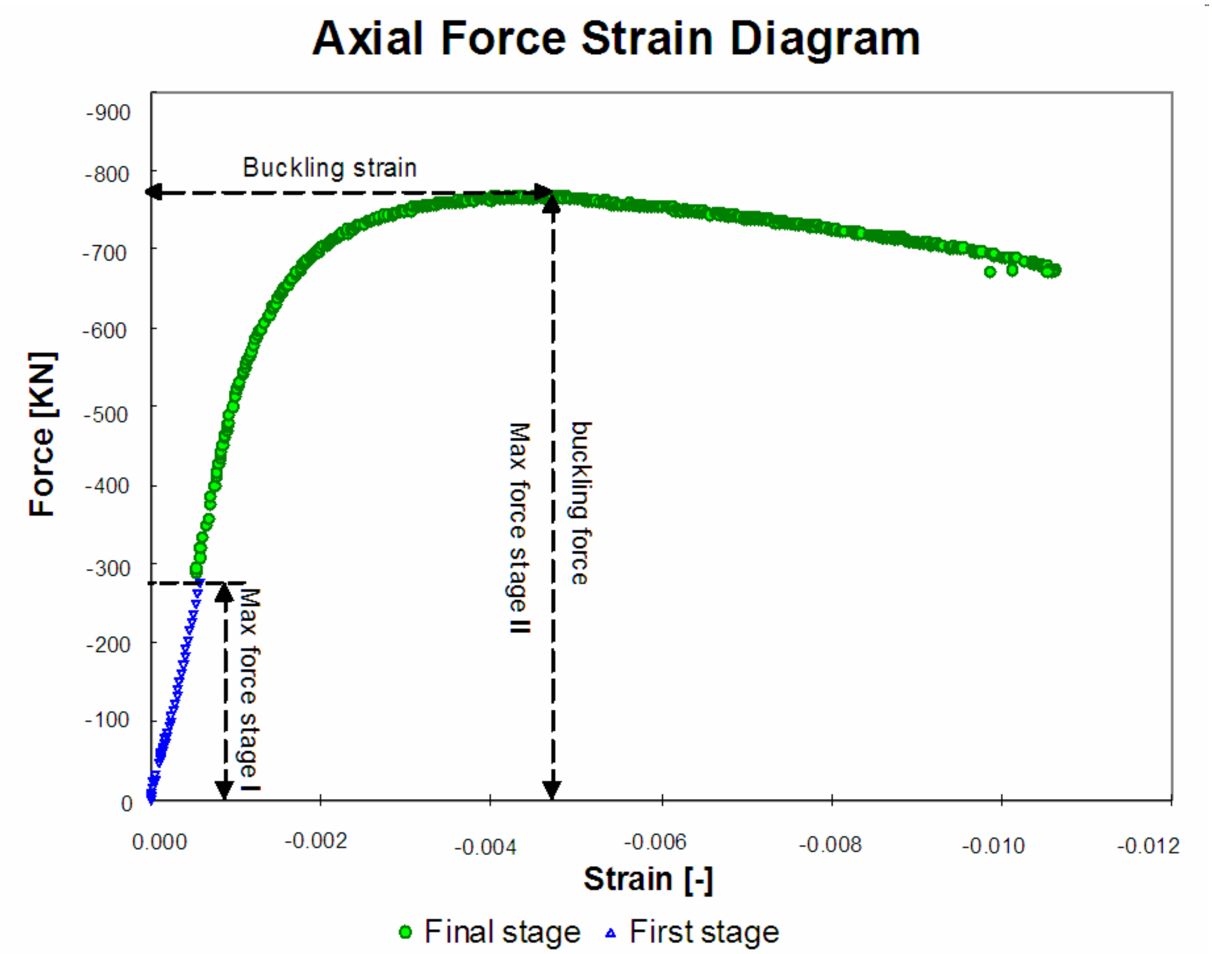

Figure 2-3: General compression diagram (extracted from test data and used as example), with stages I and II of the experimental procedure

2.4 Test Results

The six buckled liners can be seen in Figure 2-4. The buckles are axi-symmetrical and smooth in a cosine wave form and occurred gradually.

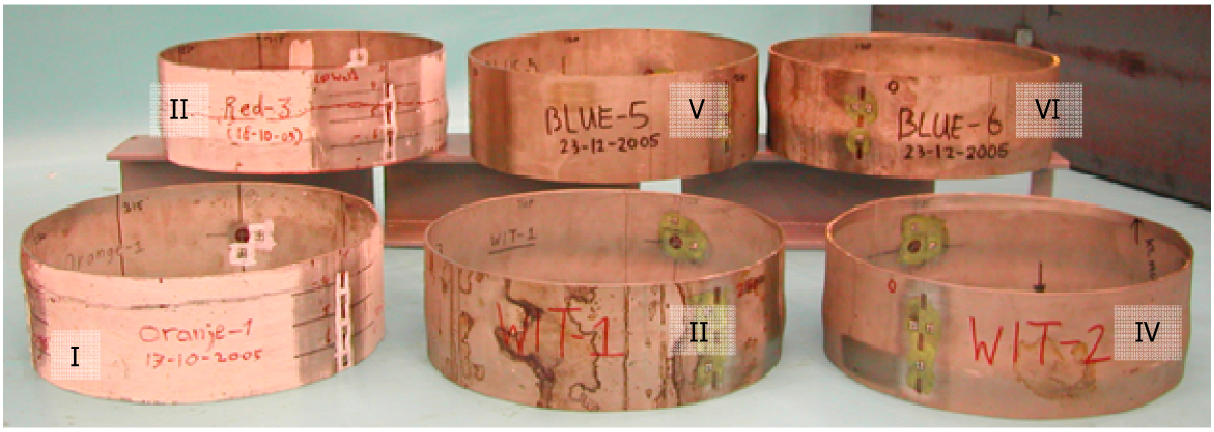

Figure 2-4: Six liner samples (I, II, III, IV, V and VI) after testing (Because of clarity the colours were altered, CRA has a grey colour.)

The buckling force and buckling strain can be found in Table 2-2. The buckles in the experiments were only deforming outwards from the centre axis of the cylinder.

Table 2-2: Buckling test data extracted from the test measurements

Test number	I	II	III	IV	V	VI
Liner test specimen name	ORANGE-1	RED-3	WHITE-1	WHITE-2	BLUE-5	BLUE-6
L [mm]	100	101	98	98	110	101
t [mm]	3	3	3	3	3	3
OR [mm]	148	148	147	147	148	148
IR [mm]	146	146	146	146	146	146
D/t	99	99	97	97	95	97
F_{max} [kN] (F_{cr})	-812	-825	-768	-770	-817	-832
ε_{cr} SG [%]	-0.38%	-0.43%	-0.46%	-0.47%	-0.35%	-0.41%
ω [mm]	42	47	47	45	42	45

The measured axial force and strain of test I to VI can also be found in Figure 2-5.

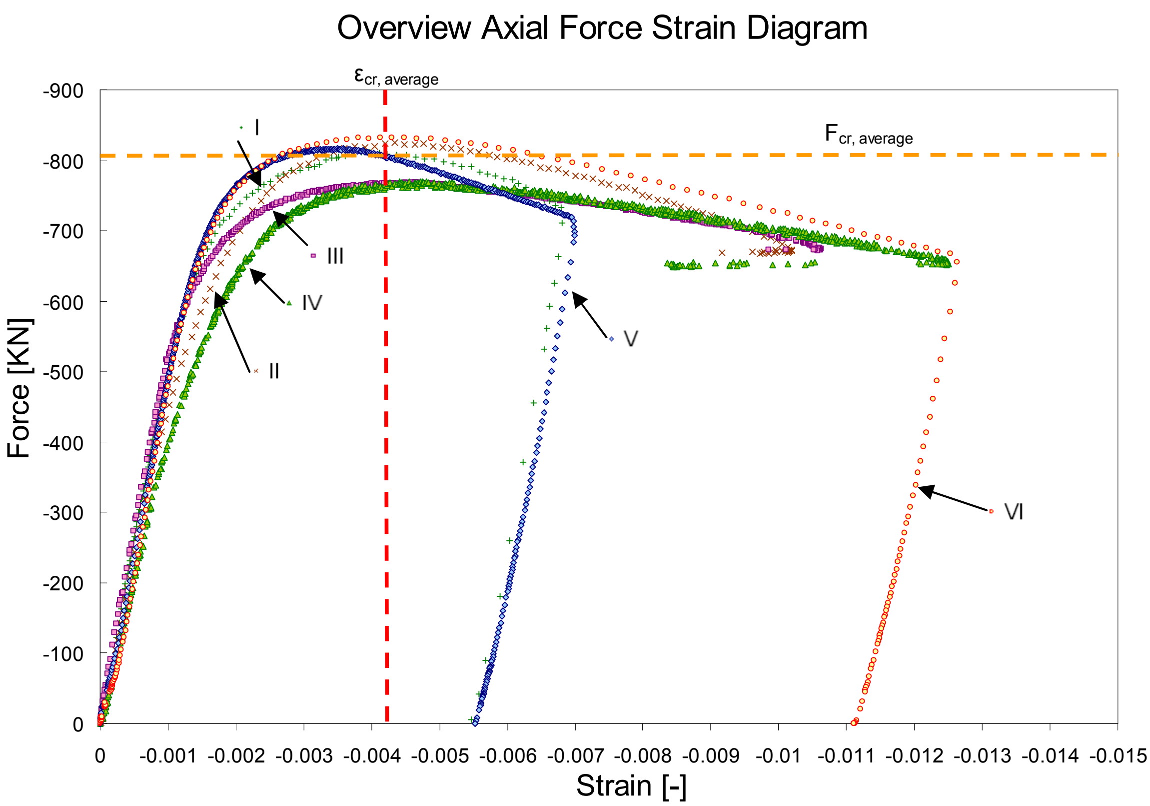

Figure 2-5: Overview Axial Force Strain Diagram of Tests I to VI of the Liner Pipe

The average critical strain, ε_{cr} at -0.0042 and average critical force, F_{cr} at 804 kN are plotted as a dotted line in Figure 2-5. Figure 2-6 is a good representation of all the liner test samples. It shows the axi-symmetrical shape of the outward buckle.

Figure 2-6: An example view of liner Red-3 just when it buckled at critical strain.

2.5 Axial Compression and Theoretical Equations

2.5.1 Subsection Introduction

In this subsection, buckling is explained with analytical equations which are then used to calculate the theoretical buckling strain of the liners which are experimentally tested. The results of the axial compression tests on the 12 ¾-inch liner will then be compared to these buckling theories

2.5.2 Theoretical Buckling Equations and Pipe Characteristics

A single wall cylinder may buckle when its surface wrinkles (buckle is a synonym for wrinkle) under the action of axial compression and thereby will undergo local or overall change in configuration. [Ref. 14 and Ref. 38]. This change in configuration or local buckling behaviour of a cylinder depends on several key parameters, such as:

-geometry,

-material characteristics,

-imperfections,

-residual stresses

-boundary conditions

[Ref. 9].

The (outer) diameter over wall thickness (D/t) ratio classifies cylinders in respect to their diameter to wall thickness. Moderately thick walled cylinders are cylinders where plastic behaviour prevails. For pipes with a D/t-ratio larger than 120, also called thin cylinders, failure occurs in the elastic range (depending on yield stress and imperfections) in an asymmetric- or diamond mode, see Figure 2-7. For pipes, with a D/t smaller than 120 (and larger than 35), moderately thick walled, plastic behaviour occurs with buckles gradually developing.

In the case of cylinders with a D/t-ratio smaller than 120 (and larger than 35), also called moderately thick and thick cylinders, local buckling occurs in the plastic range in an outward bellow, axi-symmetric failure mode [Ref. 23], see Figure 2-7. The elastic equations must first be explained to advance to the plastic equations for clarity. However, the liner samples in consideration have a D/t of ≈99 [Table 2-1] and are hereby moderately thick walled. Results of the axial compression test will thus be compared to equations for moderately thick walled cylinders, i.e. plasticity equations for plastic buckling. In plastic buckling the critical strain (strain at which the maximum stress is measured) is used as the local buckling criterion.

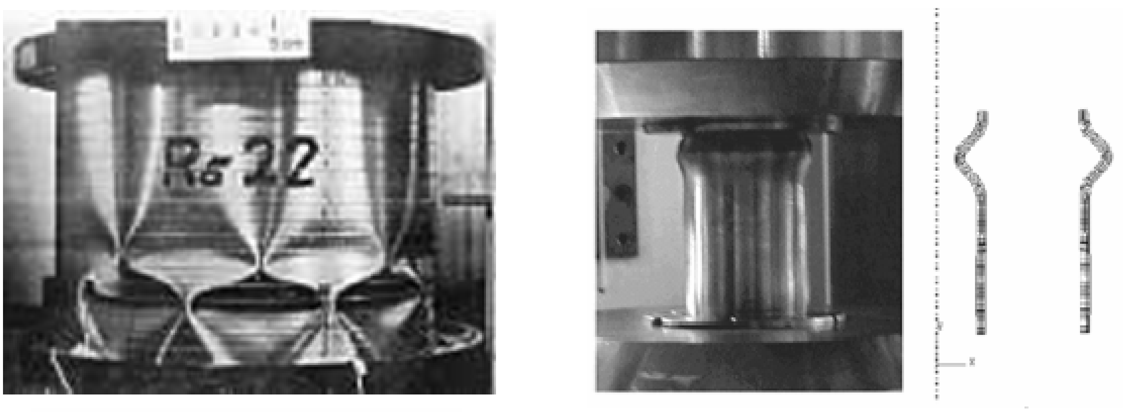

Figure 2-7: Diamond Local Buckling Mode (on the left) and Outward Bellow Mode (to the right)

2.5.3 Elastic Theory Equations for Buckling

Elastic analysis presumes linear elastic behaviour of the cylinder material, i.e. the material is obeying Hooke's law in the whole range of loading and this is shown with the Equation 2-1;

$$\sigma = E \cdot \varepsilon \qquad \text{Equation 2-1}$$

Timoshenko & Gere predicted local buckling to occur at the elastic critical local buckling stress, σ_{cr}, and elastic critical strain, ε_{cr}, with Equation 2-2 and Equation 2-3 [Ref. 38]

$$\sigma_{cr} = \frac{E}{\sqrt{3(1-\nu^2)}} \frac{t}{r} \qquad \text{Equation 2-2}$$

$$\varepsilon_{cr} = \frac{1}{\sqrt{3(1-\nu^2)}} \frac{t}{r} \qquad \text{Equation 2-3}$$

Poisson’s ratio, ν, for engineering materials usually has a value in the elastic region of between ¼ and 1/3 [Ref. 16].

The elastic local buckling deformations have a cosine wave shape in the axial direction and are defined by the half-wave length, ω [Figure 2-8]. The elastic half wave length of the buckles, ω, can be calculated using Equation 2-4. [Ref. 38]

$$\omega = 1.72 \cdot \sqrt{r \cdot t} \qquad \text{Equation 2-4}$$

Equation 2-2 and Equation 2-3 for σ_{cr} and ε_{cr} are only valid for thin cylinders of a length longer than half the wave length calculated [Ref. 38].

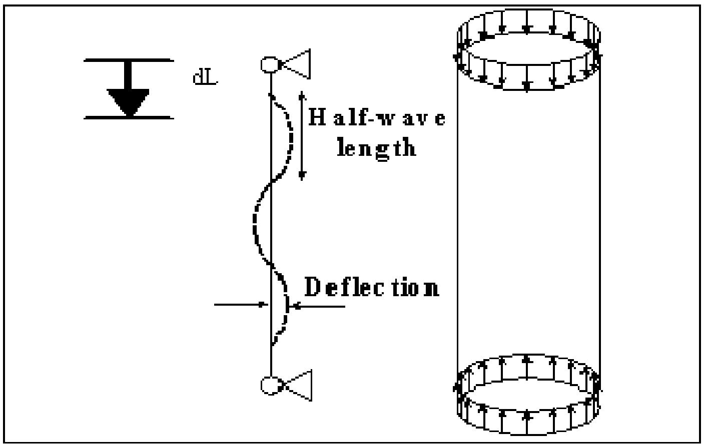

Figure 2-8: Half-Wave Length and Deflection

2.5.4 Plastic Theory Equations for Buckling

2.5.4.1 Buckling Theory by Batterman's Approach

Based on experimental observations [Ref. 40, Ref. 36], it is assumed that the prediction by the Batterman's deformation equation, is the lower bound of local buckling strain for moderately thick cylinders. Batterman's equation for the critical local buckling strain is defined in Equation 2-5.

$$\varepsilon_{Batterman,deformation} = \frac{E}{E_s} \frac{2}{\sqrt{(3((3\eta_s - 4v)\eta_t - (1-2v)^2))}} \cdot \frac{t}{r} \qquad \text{Equation 2-5}$$

Where E is the Young's modulus, E_t is the tangent modulus [Equation 2-7] and E_s is the secant modulus [Equation 2-6] [Ref. 2]

$$E_s = \frac{\sigma_{cr}}{\varepsilon_{cr}} \qquad \text{Equation 2-6}$$

and

$$E_t = \frac{d\sigma_p}{d\varepsilon_p} \qquad \text{Equation 2-7}$$

The tangent reduction factor, η_t [Equation 2-8], and the secant reduction factor, η_S [Equation 2-9], are used to simplify the notation of [Equation 2-5].

$$\eta_t = \frac{E}{E_t} \qquad \text{Equation 2-8}$$

and

$$\eta_S = \frac{E}{E_s} \qquad \text{Equation 2-9}$$

Poisson's ratio, v, in the plastic region is assumed to be ½ [Ref. 16].

Batterman defines the half-wave length of the plastic local buckle in Equation 2-10.

$$\omega_{Batterman,deformation} = \frac{1}{2} \frac{\pi\sqrt{(r \cdot t(\eta_t + 3\eta_s))}}{\sqrt[4]{(3((3\eta_s + 2 - 4v)\eta_t - (1-2v)^2))}} \qquad \text{Equation 2-10}$$

2.5.4.2 Buckling Theory by Timoshenko

The expression for the classical half wave length in case of local buckling beyond the elastic limit can be found in using Equation 2-11 [Ref. 38].

$$\omega = 1.72 \cdot \sqrt{r \cdot t} \cdot \sqrt{\frac{E_t}{E}} \qquad \text{Equation 2-11}$$

The additional factor, comparing Equation 2-4 and Equation 2-11, for the plastic range, $\sqrt{\frac{E_t}{E}} < 1$, causes the length of the waves to become shorter for local buckling beyond the elastic limit compared to the elastic Equation 2-4 [Ref. 38]. E_t is typically E/40 and E/60 for steel in general [Ref. 19].

2.5.4.3 Buckling Theory by Gerard

The critical local buckling strain according to Gerard can be found in Equation 2-12.

$$\varepsilon_{Gerard} = \frac{1}{E_s} \cdot \sqrt{\frac{E_t E_s}{3(1-\mu^2)}} \cdot \frac{t}{r} \qquad \text{Equation 2-12}$$

The factor μ in Equation 2.5-12, is given in Equation 2-13.

$$\mu = \tfrac{1}{2} - (\tfrac{1}{2} - v)\frac{E_S}{E} \qquad \text{Equation 2-13}$$

Gerard [Ref. 18] also defined the half-wave length at local buckling in Equation 2-14.

$$\omega_{Gerard,deformation} = \frac{\pi}{2\sqrt{3}} \frac{\sqrt{(\eta_t + 3\eta_s)}}{\sqrt[4]{\eta_t \eta_s}} \cdot \sqrt{r \cdot t} \qquad \text{Equation 2-14}$$

2.5.4.4 Buckling Theory by Gresnigt

Using theory and an empirical method to establish an approximation of the critical strain, Equation 2-15, was studied by Gresnigt [Ref. 20].

$$\varepsilon_{cr} = C\left(\frac{t}{r}\right)^{m} + b \qquad \text{Equation 2-15}$$

[Ref. 20].

Coefficients C, b and m are defined by experiments. For cylinders of D/t>120 Gresnigt proposed Equation 2-16 to predict the critical buckling strain whilst Equation 2-17 can be used to predict the buckling strain for cylinders with D/t<120.

$$\varepsilon_{cr} = 0.1\cdot\left(\frac{t}{r}\right) \qquad \text{Equation 2-16}$$

$$\varepsilon_{cr} = 0.25\cdot\left(\frac{t}{r}\right) - 0.0025 \qquad \text{Equation 2-17}$$

[Ref. 20].

2.5.4.5 Buckling Theory Selection

The analytical study is applied on the experiment samples and experimental data. According to Batterman the buckling strain and force as well as the wave length are independent of the length of the cylinder as long as the cylinder is longer than half the wave length [Ref. 2]. The pipe sample lengths are more than two times the half-wave length and the pipe diameter to thickness ratio, i.e. D/t-ratio, is between 90 and 120. This supports the selection of theoretical buckling equations of Gresnigt, Batterman and Gerard. The results are compared with the FEM results and experiment results in section 2.7.

2.6 Axial Compression by Finite Element Method

The finite element method (FEM) is a method where a physical system, such as an engineering component or structure, is divided into small sub regions/elements. Each element is an essential simple unit in space of which the behaviour can be calculated. This is possible by the shape functions of the elements which are interpolated from the nodal values of the elements. (The shape function is used in the equation **Ku=F**, where **K** is the stiffness matrix and is known as the shape function of an Element in FEM, **u** is the displacement vector with an entry for each node in each direction, and **F** is a vector of forces at each node of the shape function in each direction. Clearly **u** can be solved by inverting **K** to get $\mathbf{u}=\mathbf{K}^{-1}\mathbf{F}$. So shape functions relate the interior displacements of a finite element to nodal displacements approximately).

The advantage of the finite element method is that it enables the adoption of a numerical approach without introducing significant assumptions about geometry, material properties, loading conditions, deformation pattern etc.

This section will focus on establishing a FEM model in MSC.MARC for local buckling of the single 316L liner pipe, which was used in the axial compression tests.

2.6.1 Building a Finite Element Model to Simulate the Axial Compression Tests

This section will focus on the FE model made for the liner, as used in the axial compression tests. The FEM model approach is described in detail in Appendix C.

The physical and geometric properties of the 316L liner can be found in Table 2-1.

Strain hardening of the 316L liner implemented in the FEM model based on plastic strain data from tensile testing on the 316L liner material, see Figure 2-9. Figure 2-9 was used in MSC.MARC to simulate the material properties of the pipe material.

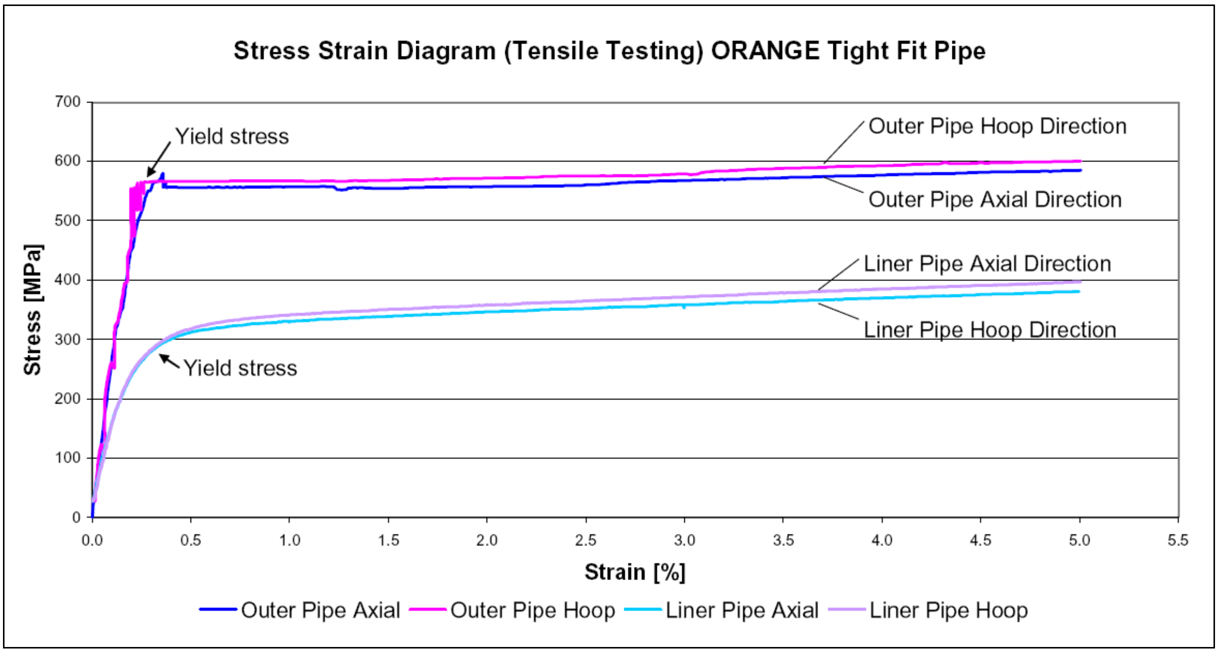

Figure 2-9: Plastic stress strain diagram from the tensile testing of 316L and the Outer pipe material, with on the x-as stress and on the y-axis strain

2.6.2 Finite Element Method Results

One Finite Element (FE) model is made from which the results will later be compared with the results of the six experiments. The critical buckling strain of the liner is obtained from the FEM model at ¼, ½ and ¾ of the liner height and can be seen in Figure 2-10. The axial buckling strain is -0.81% and the axial buckling force is -867 kN for the FE model.

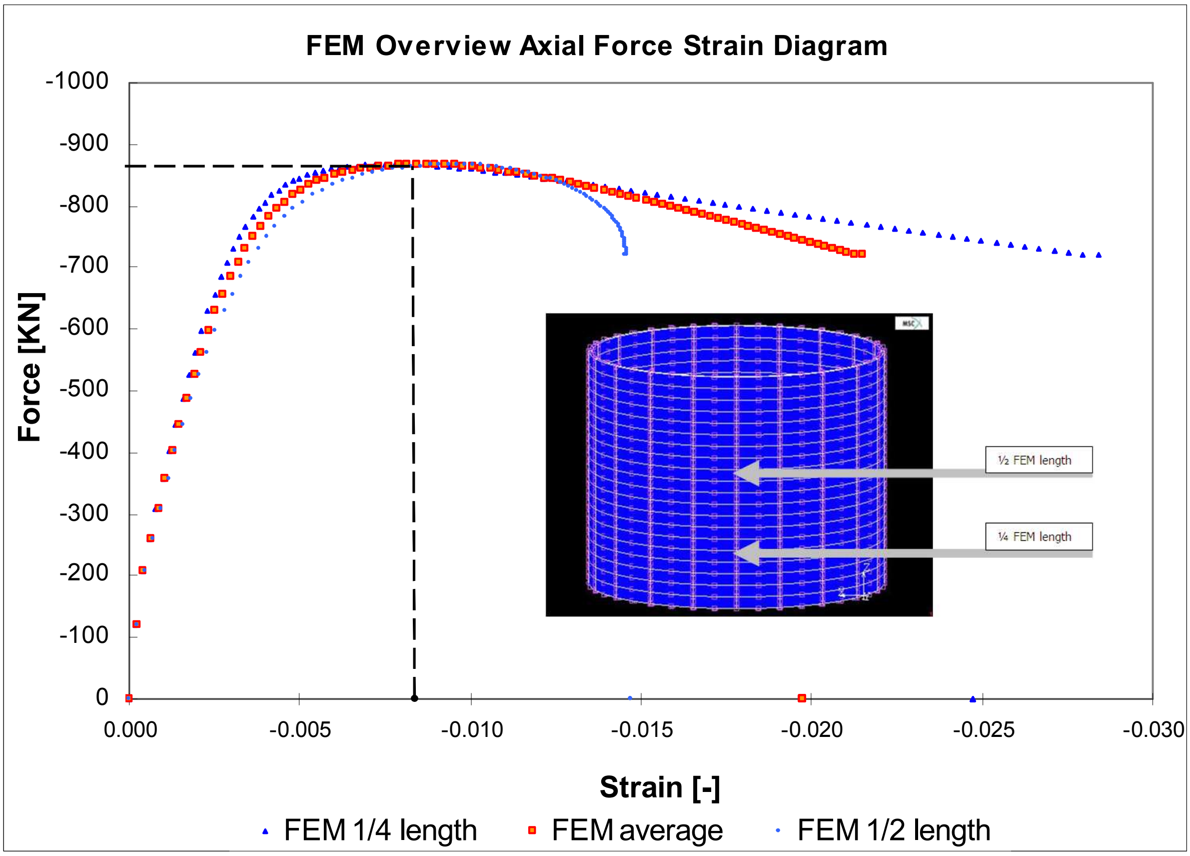

Figure 2-10: Axial force versus axial strain diagram of the FE model of the liner pipe (FEM average is the average result of the results at the locations ¼ and ½ the pipe length, see the FEM pipe illustration).

2.7 Comparison of the Experimental Results with Results of the FEM and Analytical Analysis

The general data of the test samples is shown in Table 2-3;

Table 2-3: Experiment result data for all test samples

Average test results	Liner
ε_{cr} SG [%]	-0.42%
F max [KN]	-804
ω experiment [mm]	44.7

The experiment liner data is used to calculate the analytical values using Equation 2-5, Equation 2-10, Equation 2-12, Equation 2-14 and Equation 2-17, this can be found in Table 2-4;

Table 2-4: Theoretical calculated average values of the critical strain and half the wave length for the test samples

Average analytical	Liner
ε_{cr} Batterman [%]	-0.27%
ε_{cr} Gresnigt [%]	-0.27%
ε_{cr} Gerard [%]	-0.26%
ω Batterman [mm]	43.5
ω Gerard [mm]	44.7

The FE model results can be found in Table 2-5

Table 2-5: FEM general result data

FEM Model	Liner
ε_{cr} FEM [%]	-0.81%
F max [KN]	-867
ω FEM [mm]	50

The FE model results are plotted in Figure 2-11 together with the test data of the six liners. The graphical comparison of the FE, analytical and experimental results can be found in Figure 2-12.

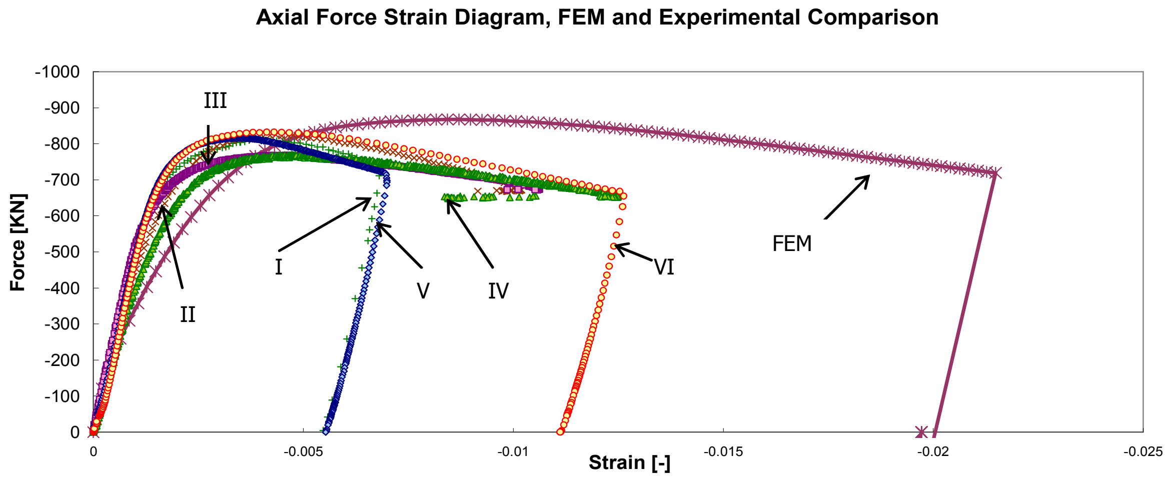

Figure 2-11: Comparison of test data and FEM average of the FEM results of the unconfined liner pipe

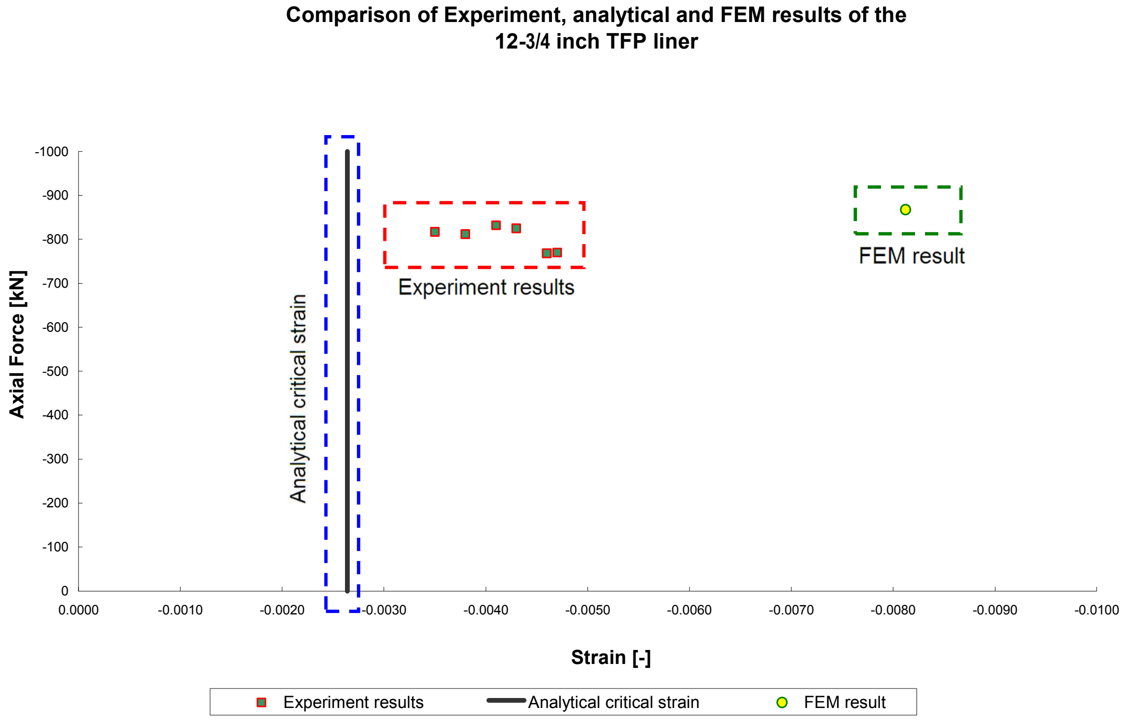

Figure 2-12: Comparison of Experiment, analytical and FEM results of the 12 3/4 inch TFP liner

Note: the straight vertical line (Analytical critical strain in figure 2.7-2) of the -0.26% strain has only a critical strain and not a related axial force, so no maximum axial force is indicated.

The comparison of the FE model and analytical data with the average experimental results can be found in Table 2-6.

Table 2-6: Average experiment, average FEM, average analytical results together with a comparison of the results of liner pipe failure in FEM with experiments and analytical with experiment.

	Averaged Data			Comparison	
type of data	Experiments (of six tests)	FEM	Analytical	Δ FEM to experiments [%]	Δ Analytical to experiments [%]
ω [mm]	45	50	44	+11.1%	-2.2%
F_{max} [kN] (F_{cr})	-804	-867	–	+7.8%	–
ε_{cr} SG [%]	-0.42%	-0.81%	-0.26%	+92.9%	-38.1%

In Table 2-6 the FE model and the analytical results are compared with the average test results for critical force and critical strain. These compare well except for the critical strain. The average FEM local buckling strain is compared to the average experimental test results and is average 92,9% larger, which indicates that the FEM results are un-conservative. The experimental results are also compared with the analytical results

It can be seen in Table 2-6 that:

a. The buckling force determined by the FEM analysis correlate well with the experiments.

b. The buckling strain determined in the FEM model is larger than the experimental value, while the analytical formula is smaller than the experimental buckling strain.

2.8 Conclusions

The difference between the Finite Element (FE) model, analytical and test results may be explained as follows.

Results from the experiments differ from the results of the FE model due to several reasons:

a. Geometrical imperfections in the Tight Fit Pipe liner in the experiments are not taken into account in the FE model. Geometric imperfections, which were not used in the FE model, can be:
   - Longitudinal girth welds of the liner,
   - Local or global ovality of the liner,
   - Local increase or decrease of wall thickness.

b. Material discontinuities along the pipe, which are not taken into account in the FEM model. Material discontinuities, which were not used in the FE model, can be:
   - Discontinuities of material strength, different young's modulus, Poisson's ratio, etc.,
   - Contamination by other materials in the liner material, e.g. a nickel lump in the liner wall.

c. Side effects of the axial compression apparatus was also not taken into account in the FEM model and these can influence the compression speed, which is gradual and hereby idealist in the FE model. Side effects of the apparatus, which were not used in the model, can be:
   - Vibrations of the installation when compressing the liner,
   - Off centre loading of the liner.

d. The FEM boundary conditions will also influence the FEM model results. FEM boundary conditions, which were not used in the FE model, can be:
   - Friction forces between the liner and the compression pad due to movement,
   - Influence and interaction of different boundary conditions at both ends of the liner.

Results from the experiments differ from the results of the analytical calculations due to several reasons:

e. The wave lengths of the FEM model are also compared with the experimental results and they compare well. Note that the wavelengths of the liners was difficult to measure at the moment of critical local buckling strain.

f. All analytical equations should be considered as the lower bound criteria. The equations are design formulae and should be considered conservative, compared to the test and FEM data.

The FEM data is the most "optimistic" or upper bound, because it does not account for imperfections and local discontinuities in the material. The experimental data falls between the conservative analytical and the upper bound FEM data. This is as expected.

3 Axial Compression of the Liner Pipe in a 12 ¾-inch Outer Pipe

3.1 Introduction

The Tight Fit Pipe (TFP) consists of an inner liner and an outer pipe. The TFP has an outer diameter of 12 ¾-inch. This 12 ¾-inch TFP is used in the experiments and the properties are as follows.

The liner pipe is made of 316L material which is a corrosion resistant alloy (CRA). The outer pipe is made of API 5L X65 steel, a high grade steel often used in the pipeline industry. The 316L liner and the outer pipe both have a longitudinal weld. The outer pipe is an U-ing, O-ing and Expanded pipe (UOE pipe); the longitudinal weld is made by electric resistance welding (ERW pipe). The material and geometric properties of the 316L liner pipe and the API 5L X65 pipe can be found Table 3-1;

Table 3-1: TFP geometry and material properties

	Outer diameter	Wall thickness	Average Liner length	Modulus of Elasticity (E)	0.2 % yield strength	Poisson's ratio (ν)
[Unit]	[mm]	[mm]	[mm]	[MPa]	[MPa]	[-]
Liner	296	3.0	100	193000	305	0.3
Outer pipe	324	14	100	200000	448	0.3

3.2 Procedure of Experiments

The TFP (shown in Table 3-1) has been used in the experiments to analyse the buckling behaviour of the liner when confined and pre-stressed inside the outer pipe as fabricated by the thermo-hydraulic manufacturing process (explained in detail in Appendix A). The influence of circumferential the pre-stress on the buckling behaviour of the liner in the TFP is investigated by using two types of TFP pipes;

I. High compressive hoop stress in the liner (also called high fit)

II. Low compressive hoop stress in the liner (also called low fit)

Pipes with two different values of circumferential pre-stress have been tested, 199 MPa for high fit and 53 MPa for low fit of the liner in the 12 ¾-inch TFP.

1. The first objective of the experiments is to establish the influence of the buckling strength (buckling strain and force) by positioning the liner pipe inside the outer pipe.

2. The second objective is to determine the influence of high or low fit on the buckling strain and force of the liner while confined in the outer pipe.

Only the liner pipe is axially compressed by the same axial compression machine as used for the single liner pipe by a compression pad that exactly fits the liner, but does not axially compress the outer pipe. The setup of the compression apparatus is explained in detail in Appendix D. The TFP with the compression pad applied can be seen in Figure 3-1.

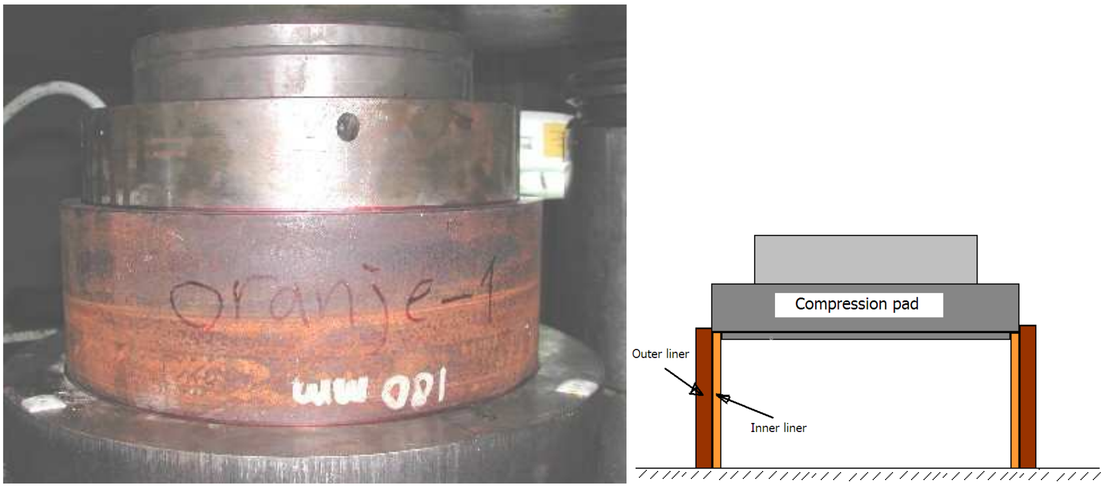

Figure 3-1: TFP with compression pad (drawing right is a schematic cutaway representation of the photo left)

The TFP samples are machined at the outer ends to create an even compression surface. At one end the liner is slightly machined and hereby less long than the outer pipe to accommodate the compression pad. This accommodation is to avoid nonalignment of the pad. Twelve axial strain gauges were attached to the liners. The strain gauges (SG) are placed from top to bottom (¼, ½ and ¾) of the liner height at:

- 0° degrees with strain gauge SG-1, SG-2 and SG-3
- 90° degrees with strain gauge SG-4, SG-5 and SG-6
- 180° degrees with strain gauge SG-7, SG-8 and SG-9
- 270° degrees with strain gauge SG-10, SG-11 and SG-12

These SG locations on the Tight Fit Pipe can be seen here in Fig 3.2-2.

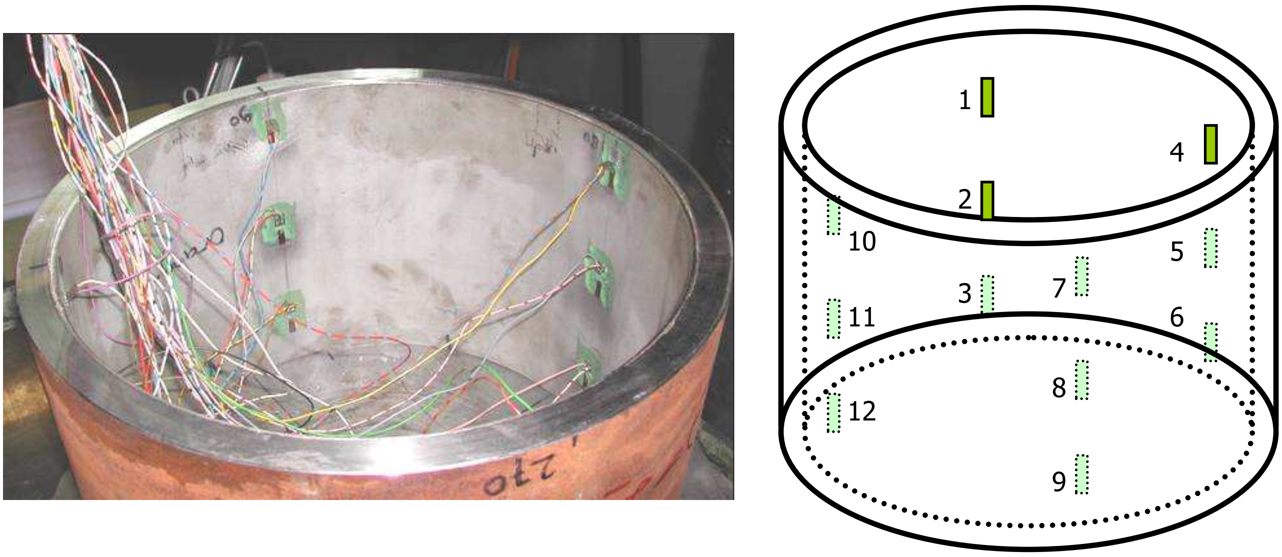

Figure 3-2: Strain gauges configuration on the TFP samples

The axial compression experiments of the liner consist of two stages:

I. The first stage consists of building up an axial force to 300 kN to remove any play or leeway in the setup. The force remains within the elastic range (strain < 0.002 (Ref. 38)) such to cause no permanent deformation of the liner. The force is then released gradually to zero.

II. In stage two the force is increased until liner buckling occurs. The buckling force in the axial compression tests is identified as the maximum force that could be applied onto the test specimen. The buckling strain is defined as the strain measured at the highest critical force. Critical force is the maximum force which a pipe can hold.

3.3 Comparison of The Liner Pipe with & without the 12 ¾-inch Outer Pipe of the Tight Fit Pipe

The liner from the 12 ¾ inch Tight Fit Pipe can be seen as a single wall pipe. Single wall buckling is mainly axi-symmetrical as can be seen in the experiments of Chapter 2 (Axial Compression of only the Liner Pipe of a 12 ¾-inch Tight Fit Pipe). The tests show that the liner confined in the Tight Fit Pipe buckles inward and buckles a-symmetrical.

The liner has a higher capacity in force and strain when the liner is placed with a residual circumferential pre-stress in the liner, i.e. mechanical fit compared with the liner alone. This effect can be seen in Figure 3-3, the red dotted line of Liner test specimen VI (Blue-6) has significant less capacity than all other lines in the figure of the liners confined in an outer pipe.

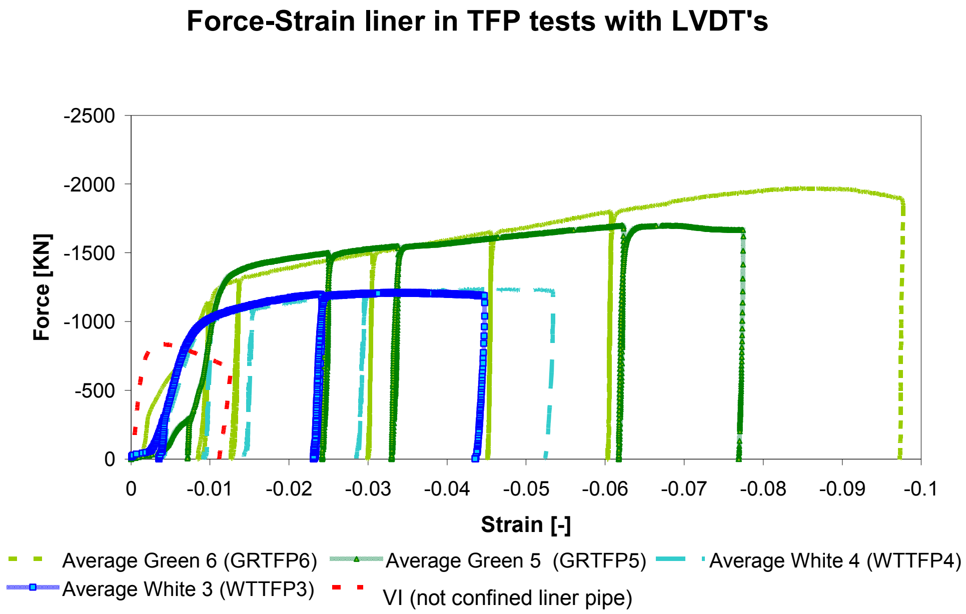

Figure 3-3: Force-strain diagram of liners confined in the outer TFP pipe, VI liner is not confined.

3.4 Comparison of the Results of Test on Low and High Residual Hoop Stress Tight Fit Pipe

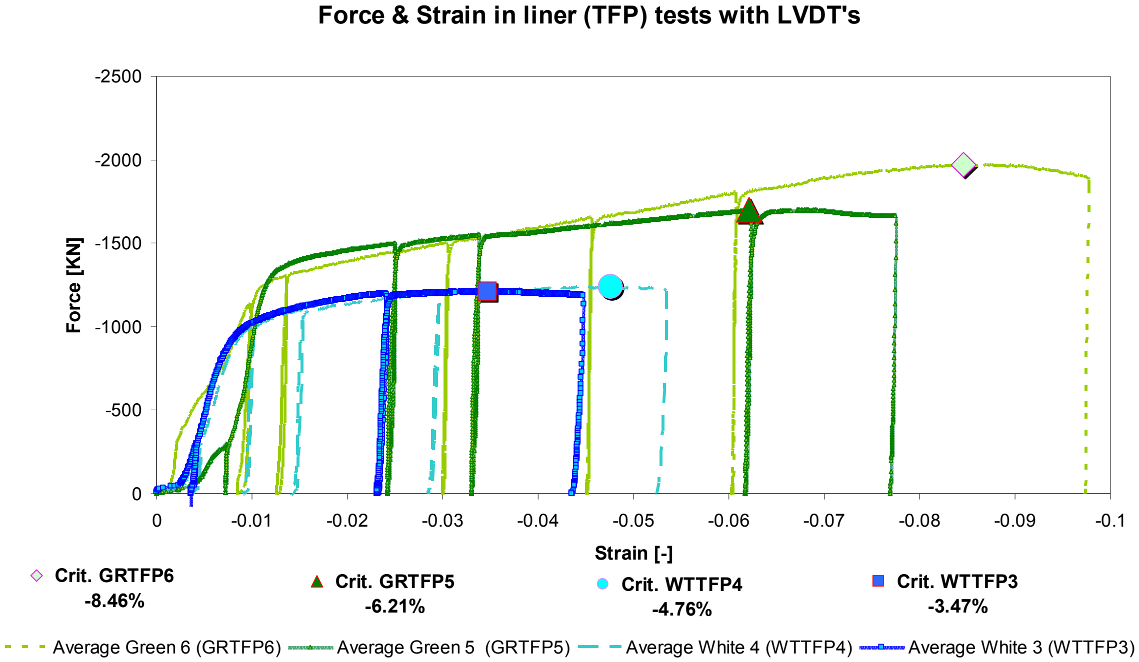

Figure 3-4: Force-strain diagram of liners confined in the outer TFP pipe

A comparison of Tight Fit Pipes with high and low compressive hoop stress in the liner can be seen in Figure 3-4. It shows the Tight Fit Pipe (TFP) experimental test data of four tested TFP's. GRTFP5 (a.k.a. TFP Green 5) and GRTFP6 (a.k.a TFP Green 6) are high fit TFP's, WTTFP3 (a.k.a. White 3) and WTTFP4 (a.k.a. TFP White 4) are low fit TFP's.

3.4.1 Axial Compression of the Liner in the TFP

The experiments showed the following:

a. Inward buckles of the liner in pipe, which were not axi-symmetrical (shown in Figure 3-5).

b. The location and size and measured strain of the wrinkle during the test was not predictable. The buckles were first small, and could only be felt by the use of fingertips and were not easily visible. The small buckles gradually grew in size and no sharp or fast growth was seen, when applying more force and strain.

c. The final buckle shape was mostly elliptical and not covering more than 90 degrees of the total 360 degrees circumference. The length (in circumferential direction) was from 25 mm up to 120 mm of the inner circumference of the liner. The longitudinal wave length was from 15 mm up to 40 mm.

d. The liner buckles initiated and where most severe at the location of the outer pipe longitudinal weld. These buckles preceded more buckles which formed at other locations. The number of buckles was between one and six and with different size and shapes. Most liners showed one or two big buckles and a few small.

e. The liner of the high fit Tight Fit Pipe (TFP) had more strength (higher maximum strain at higher maximum Force) compared to the liner of the low fit TFP pipes.

f. Large buckles were generated at the location of the outer pipe longitudinal weld and smaller buckles on other places, but almost none at the liner weld (near to 90 degrees offset to the outer pipe weld). The liner weld seems to be a stiff point in the liner were buckles do not tend to form.

g. The outer pipe longitudinal weld seems to initiate a-symmetrical buckling of the liner.

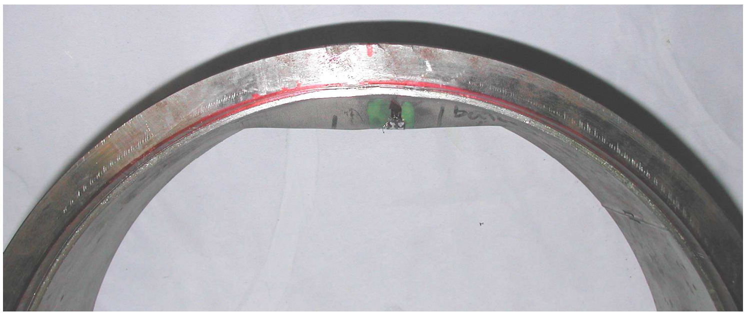

Top View of the liner and outer pipe wall of the Tight Fit Pipe

Same Tight Fit Pipe as above but at a different viewing angle, the inside of the TFP.

Figure 3-5: Inner liner view at the outer weld location of a buckle

Figure 3-6 and Figure 3-7: Cross-section view of Green 5 and 6 TFP specimen after testing show four TFP pipes of which the first has a low fit and the second a high fit.

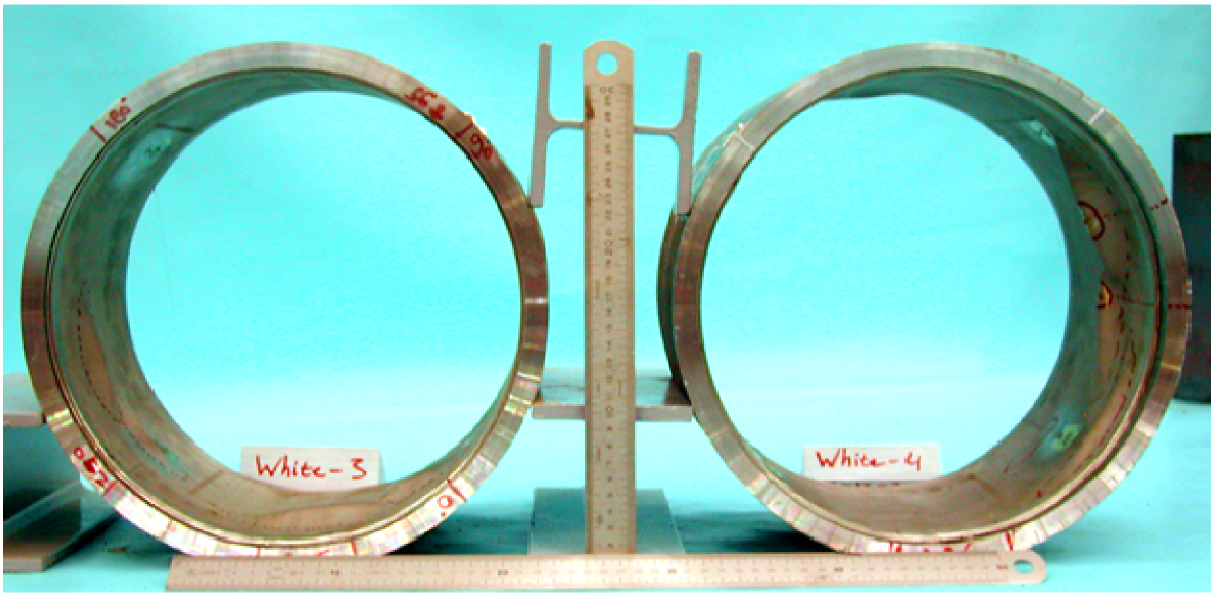

Figure 3-6: Cross-section view of White 3 and 4 TFP specimen after testing

White 3 (WTTFP3) and 4 (WTTFP4) are TFP specimens with a "low" residual hoop stress of 59 MPa (N/mm^2).

Figure 3-7: Cross-section view of Green 5 and 6 TFP specimen after testing

Green 5 (GRTFP5) and 6 (GRTFP6) are TFP specimens with a "high" residual hoop stress of 199 MPa (N/mm^2).

3.4.2 Remotely Controlled Laser Trolley (local ID pipe scanner)

Ir. Kees van Beek (University staff) of the STEVINLAB, made a custom built remotely controlled robot to measure the inner radius of a pipe. This robot laser trolley is called Pluto from this point onward, and is shown in Figure 3-8.

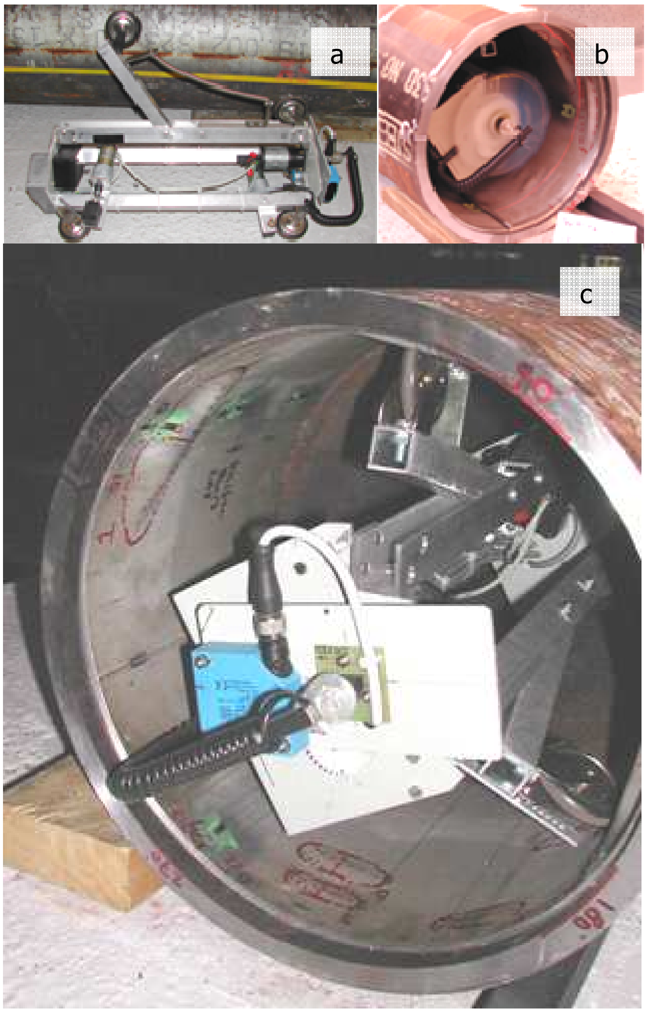

a (top left): side view

b (top right): scanning the inside (rotating laser) of a Tight Fit Pipe (TFP).

c (bottom): the "head" of Pluto, stationary in a TFP (with rotating laser and receiver/recording eye)

Figure 3-8: Pluto the local inner radius scanner (shown in a, b and c)

The measuring laser is fixed on a rotating head and mounted on a self propelled vehicle which is directed by a computer program. The program records the ID at different angle and this is done at consecutive pipe intervals, e.g. every 5 millimetre. It is possible to plot the inner pipe geometry, after processing this data in MATLAB(⇧), this can be seen in Figure 3-9.

Note (⇧): MATLAB is a programming tool for numerical computations with matrices and vectors.

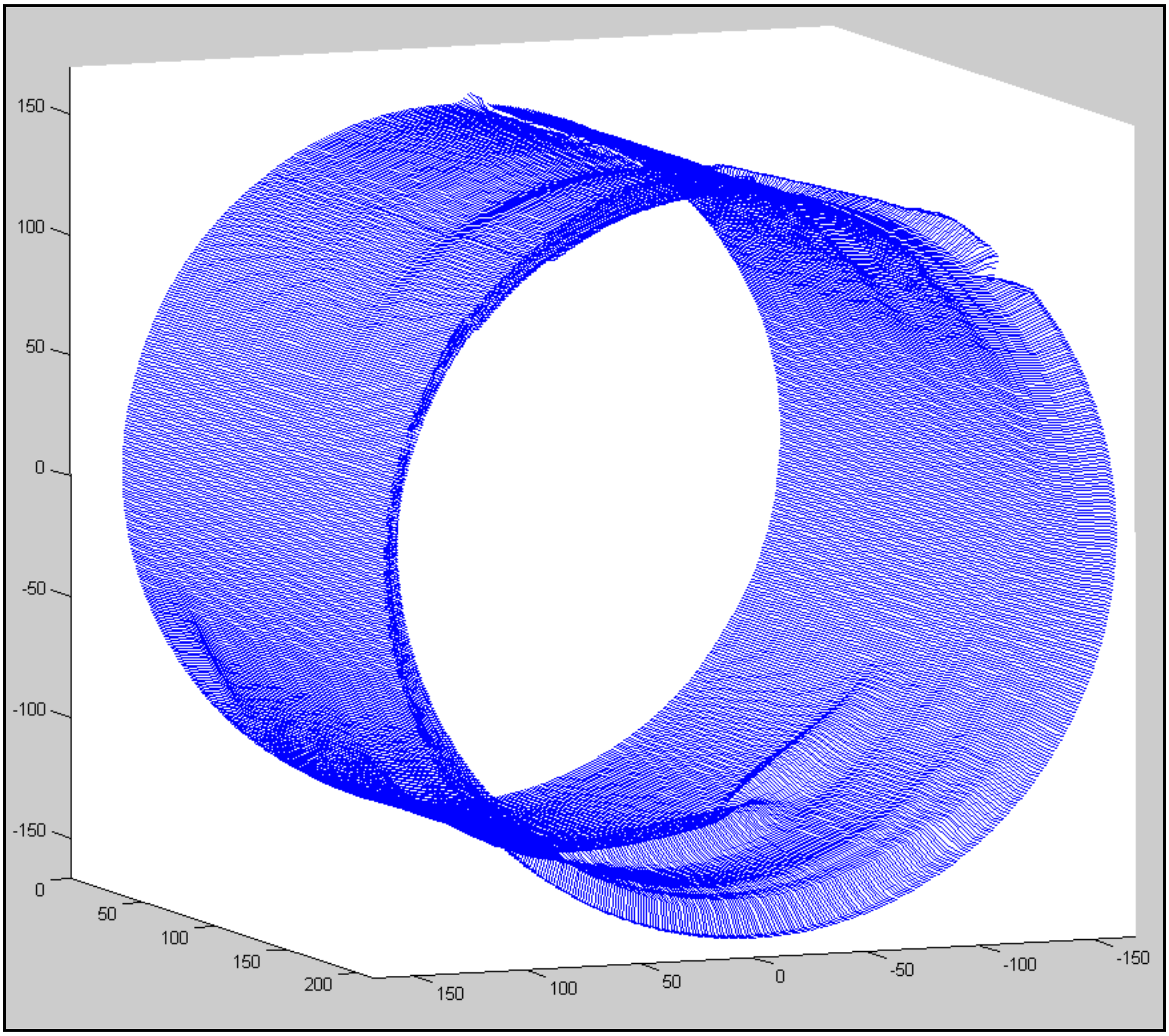

Figure 3-9: 3D Liner PLUTO Data Processed with MATLAB. (TFP White 4)

The processed 3D PLUTO data of TFP liner Orange 1, Orange 5, Green 6, White 2 and White 4 can be seen in Appendix E. The wrinkles of the buckled liner are clearly visible. The representation is only the surface. The liner thickness is not measure and but assumed to be unchanged.

3.5 Conclusions

The experiments have shown that:

a. The longitudinal outer pipe weld is the initiator of the first buckles in the liner pipe. This is predominant in the high residual hoop stress pipes.

b. The occurrence of small initial wrinkles in the liner of the Tight Fit Pipes during the test located at the Tight Fit Pipe longitudinal weld may be explained by the fact that the presence of the weld with an irregular surface or an initial imperfection, resulted in a less even distribution of the contact stress between the liner and the Tight Fit Pipe.

c. The tests of the liner pipes show that residual hoop stresses (high fit and low fit) have a significant influence on the critical buckling strain and stress as shown in the increase of buckling force and strain of the high fit liners compared with the low fit liners.

4 Conclusion and Recommendations

4.1 Conclusions

a. Buckling of the liners (of TFP pipes used in the experiments), without the outer pipe, occurred outward in a single axi-symmetrical wrinkle.

b. The liners in the tight fit pipes, confined in an outer 12 ¾ inch pipes used in the experiments, buckle inward in a non-symmetrical wrinkle.

c. Wrinkles (of liners confined in an outer 12 ¾ inch pipe) do not exceed 90° of the circumference. The wrinkles have an axis which is circumferential. Wrinkles do not tend to connect with each other if more than one is present at about the same height.

d. The maximum force in the load - strain diagram was considered to be the point at which wrinkling occurred. There was a good agreement between the Finite Element results and test results for the maximum force. The FEM results for the strain at the maximum force were much higher than in the tests.

e. Buckling of a liner in a 12 ¾ inch pipe has a larger critical buckling force than a liner which is not confined in an outer pipe. This is due to the resistance to outward buckling. Bigger wrinkles must fit in a smaller radius which costs more energy than free outward buckling. This could also be the reason why the wrinkles do not tend to form as one big wrinkle in a 360 degrees radius. Outward buckling tend to occur in one axi-symmetrical wrinkle.

f. The buckling behaviour of the liner in the TFP is believed to be influenced by three different TFP properties:

1 Low or high fit (Magnitude of the residual hoop stress in the line).

2 Type of CRA material used in the liner (Material strength).

3 Type of outer pipe used, seamless or UOE-pipe (Liner to outer pipe contact irregularities)

f.1 has been proven in the test results; f.2 and f.3 are still to be proven in future work.

.

4.2 Recommendations for Future Work

For improved Testing:

1 The use of real-time camera's inside the pipe is recommended for future work. Camera's, shown the buckling development with respect to time, strain and axial compression will be a excellent tool to improve understanding of buckling behaviour.

Stopping the test sequence to check the liner for buckling can be avoided. This will have effect on the whole experiment, because unloading and re-compressing the test specimens can alter the configuration and is not simple to replicate.

For an Improved FEM model:

2 The following is a recommendation for future work in modelling and comparing FEM results to experimental tests. A scan with, for example PLUTO (ID-scanner), can be made of the pipe before and after experimental testing. The scans may be used in a Finite Element (FE) program to generate a geometry with the imperfections (dents and bulges) and exact pipe dimensions (pipe ovality).

A FEM model with identical properties (e.g. material unconformities) and pipe geometry (a 3D-scan) from a test specimen will give less discrepancies between experimental and FEM results. This will give a better prediction of buckling force and strain.

For better and further advanced understanding of behaviour of buckling of the liner of the TFP:

3. Tests with different CRA materials, with different material properties

4. Tests with seamless inner liner and outer pipe to compare with pipes with a weld seam.

5. Tests with spirally welded pipes to compare with longitudinally welded pipes and seamless pipes.

6. Tests that axially compress the integrated TFP (inner liner with outer pipe)

5 References

Ref. no.	**Name of Originator** (Year of Publication.) *Title*, Print details
Ref. 1	**American Bureau of Shipping** (2005) Commentary on the guide for Local buckling and ultimate strength assessment for offshore structures, March 2005.
Ref. 2	**Batterman, S.C.** (1965) Plastic Buckling of the Axially Compressed Cylindrical *Shells* AIAA Journal 1965 Vol. 3 (2): 316-325 and Vol. 3 (9): p.1792.
Ref. 3	**Bouwkamp, J.G** (1975), Local buckling and Post-Local buckling Strength of Circular Tubular Cylinders, OTC 2204
Ref. 4	**Bushnell** (1985), D., *Computerised Local buckling Analysis of Shells,* Martinus Nijhoff Publishers, Dordrecht, 1985.
Ref. 5	**Cook , R. D. , Malkus, D. S. and Plesha, M. E.** (1989),*Concepts and applications of finite element analysis*, John Wiley & Sons, Third edition 1989.
Ref. 6	De Koning, A.C., Nakasugi, H. and Li Ping (2004) *TFP and TFT Back in Town (Tight Fit CRA Lined Pipe and Tubing)* Stainless Steel World, January/ February 2004, p.53-61
Ref. 7	**Donnell, L.H.** (1933), Stability of Thin-Walled Tubes under Torsion, NACA 479
Ref. 8	**Eaton, W P, Bitse F, Smith J H, Plummer D W** (1999),A new analytical solution for Diaphragm Deflection and its application to a surface-micromachined pressure sensor, ICMSM 1999
Ref. 9	**ESDEP** (1995)-*The European Steel Design Education Programme* – lecture chapter (A) 8.7. and (B) 8.8
Ref. 10	**Esslinger** (1969), M. T., and Geier, B. M., *Local buckling and Post Local buckling Behaviour of Thin-Walled Circular Cylinders*, International Colloquium on Progress of Shell Structures in the last 10 years and its future development, Madrid, 1969.
Ref. 11	**European Standard** (2004), Eurocode 3: design steel structures, Part 1-6: strength and stability of shell structures, October 2004.
Ref. 12	**Focke, E. S.** (2004), Experimental Research on Local buckling Behaviour of Tight Fit Pipe™
Ref. 13	**Focke, E. S.** (2007), *Reeling of Tight Fit Pipe*, TU Delft PhD Thesis 2007
Ref. 14	**Flügge (**1967), W., "Stresses in Shells", Springer-Verlag, New York, 1967.
Ref. 15	**Gerard, G.** (1956), Compressive and Torsional Local buckling of Thin Walled Cylinders in the Yield Region, NACA TN 3726
Ref. 16	**Gerard, G. and Becker, H.** (1957-A), Handbook of Structural Stability Part I – Local buckling of Flat Plates, NACA TN 3781
Ref. 17	**Gerard, G. and Becker, H.** (1957-B), Handbook of Structural Stability Part III – Local buckling of Curved Plates and Shells, NACA TN 3783
Ref. 18	**Gerard, G** (1962). On the role of initial imperfections in plastic local buckling of cylinders under axial compression. Journal of Aerospace Science 1962;29:744–5.
Ref. 19	**Gresnigt, A.M.** (1985), Kritieke Stuik en Kritieke Rotatie in verband met Plooien van Stalen Transportleidingen, IBBC-TNO, OPL 85-343
Ref. 20	**Gresnigt, A.M.** (1986), *Plastic Design of Buried Steel Pipelines in Settlement Areas*, HERON, Volume 31, No.4, ISSN 0046-7316
Ref. 21	**Gresnigt, A.M. and van Foeken, R.** (2001) *Local Buckling of UOE and Seamless Steel Pipes* Proceedings of the Eleventh International Offshore and Polar Engineering Conference, Stavanger, Norway
Ref. 22	**Hauch, S., Bai, Y. and Kenny, J.P.** (1998), *Use of finite element analysis for local buckling design pipelines*, 17th International Conference on Offshore Mechanics and Arctic Engineering 1998, OMAE98-3907.

Ref. no.	**Name of Originator** (Year of Publication.) *Title*, Print details
Ref. 23	**Bai Damsleth** (?) "Design through analysis applying Limit-state Concepts and reliability methods"
Ref. 24	**Hoefakker , J.H. and Blauwendraad, J**. (2003), *Theory of Shells*, Sections Structural Mechanics, Faculty of Civil Engineering and Geosciences, Delft, The Netherlands
Ref. 25	**Kato, B.** (1977), *Local buckling of Steel Circular Tubes in Plastic Region*, Proc. Int. Colloquim on Stability of Structures under Static and Dynamic loads, SSRC/ASCE, Washington
Ref. 26	**Krivetsky, A.** (1955), Plasticity coefficients for the Plastic Local buckling of Plates and Shells, J. Aero. Sci., Vol.22, pp.432-435
Ref. 27	**Lee, L.H.N.** (1962) Inelastic Buckling of Initially Imperfect Cylindrical Shells *Subject to Axial Compression* Journal of the Aerospace Sciences, January, pp.87-95
Ref. 28	**Lubarda, Vlado A.** (2001), *Elastoplasticity theory* CRC Press LLC,ISBN 0-8493-1138-1
Ref. 29	**MARC** (2001) *Introductory Course 2001* MSC. Software Corporation
Ref. 30	**Murphy, C.E.** (1975), *Ultimate Pipe Strength under Bending, Collapse and Fatigue*, Shell development Company, Pipeline R&D Laboratory, deepwater Pipeline feasibility Study, section 21-1, Houston
Ref. 31	**Nachbar, W. and Hoff, N.J.** (1962), The Local buckling of a Free Edge of an Axially Compressed Circular Cylindrical Shell, Quart. Appl. Math., Vol.20, No.3, pp.267-277
Ref. 32	**Ore E, Durban D** (1992). *Elastoplastic local buckling of axially compressed circular cylindrical shells*. International Journal of Mechanical Sciences 1992;34(9):727–42.
Ref. 33	**Popov, E.P., Sharifi, P. and Nagarajan, S**. (), Inelastic Local buckling Analysis of Pipes Subjected to Internal Pressure, Flexture and Axial Loading, , pp.11-23
Ref. 34	**Samson Y, Seong-Gu H, Soon-Bok L, Bong-Soo K** (2003). *Low cycle fatigue testing of 429EM stainless steel pipe*. International Journal of Fatigue 2003;25:1301-07
Ref. 35	**Seide P. and Weingarten, V.I.** (1961), *On the Local buckling of Circular Cylindrical Shells under Pure Bending*, Journal of Applied Mechanics, Vol.28, No.1, pp.112-116
Ref. 36	**Sobel LH, Newman SZ** (1980). *Plastic local buckling of cylindrical shells under axial compression*. Journal of Pressure Vessel Technology 1980;102:40–4.
Ref. 37	**Suer** (1958), **H.S., Harris, L.A., Skene, W.T. and Benjamin, R.J**. (1958), *The Bending Stability of Thin-Walled Unstiffenend Circular Cylinders Including the Effects of Internal Pressure*, Journal of the Aeronautical Sciences, Vol.25, No.5, pp.281-287
Ref. 38	**Timoshenko, S. & Gere**, J.M. (1963), *Theory of Elastic Stability*, McGraw-Hill Book Co., ISBN 0-07-085821-7
Ref. 39	**Timoshenko** (1959), S. and Woinowsky-Krieger, S., *Theory of Plates and Shells*, McGraw-Hill, New York and Kogakusha, Tokyo, 1959.
Ref. 40	**Yamaki N** (1984). *Elastic stability of circular cylindrical shells*. New York: North-Holland; 1984.
Ref. 41	**Yoshida, T., Matsui, S., Atsuta, T., Hasegewa, H., Kakehi, K., Iwase, T. and Kuboyama, K**. (1986) *Mechanical-Bonded Double-Wall Pipe for Severe Corrosion Environment* Evaluation Materials Conference KOBE

Appendix A

The manufacturing process is explained to show where and how the residual stress is "developed" in the Tight Fit Pipe, TFP. A schematic overview is given of the TFP manufacturing process by a cross-section diagram (see Figure Appendix A-1)

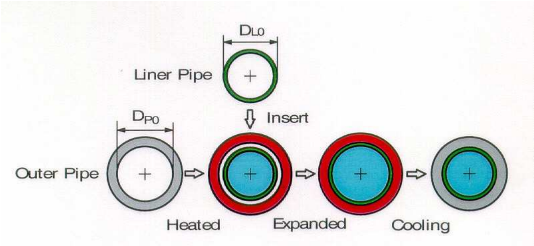

Figure Appendix A-1: Tight Fit Pipe™ cross-section during the manufacturing process [Ref. 41]

This Appendix will only discuss the influence of the manufacturing process on the TFP, without going into detail into the equipment used.
The residual hoop stress in the inner liner and the outer pipe is a result of the TFP manufacturing process. The residual compressive hoop stress of the liner is called the gripping force and is also called the mechanical fit. This gripping force is mainly influenced by the plastic deformation of the inner liner and the thermal shrinkage, after thermal expansion of the outer pipe.

The different stages of the manufacturing process, which are explained from stage 1 to the final stage, stage 7 are also supported graphically in Figure Appendix A-2 to Figure Appendix A-5

Stage 1: Cooling of the Liner Pipe (Figure Appendix A-1)

The liner pipe is assumed to be initially at room temperature at the beginning of the manufacturing process. As soon as the hydraulic expansion machine (which is also a cooling machine) is inserted into the liner pipe, the liner pipe temperature cools down from the room temperature, assumed 297 K (25°C), to the temperature of the cooling water.

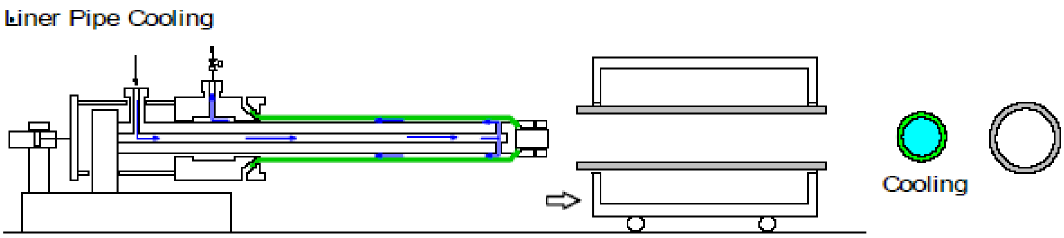

Figure Appendix A-2: Stage 1, Cooling of The Liner

Stage 2: Heating of the Outer Pipe (Figure Appendix A-3)

The outer pipe is heated from room temperature assumed 297 K (25°C) to the maximum temperature of the outer pipe. This maximum is the oven temperature.

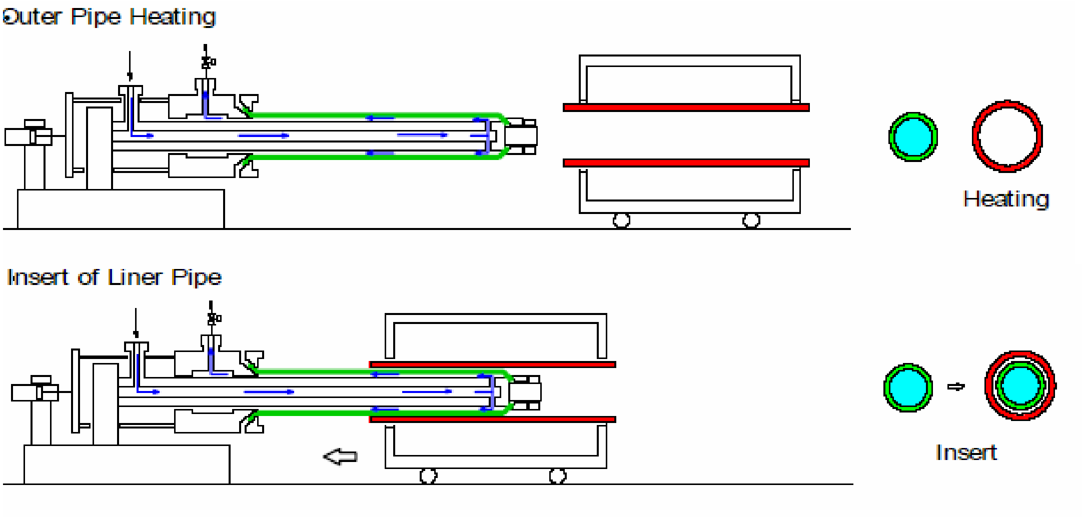

Figure Appendix A-3: Stage 2, Heating of the outer pipe and cooling of the inner pipe

Stage 3: Expanding the Liner Pipe with Hydraulic Internal Pressure Maximum Internal Pressure is Reached (Figure Appendix A-4)

The internal overpressure is created by the internal hydraulic pressure of the cooling water. The liner pipe is hydraulically expanded until yield, during the pressure increase, to maximum pressure, the liner expands plastically and makes contact with the outer pipe.

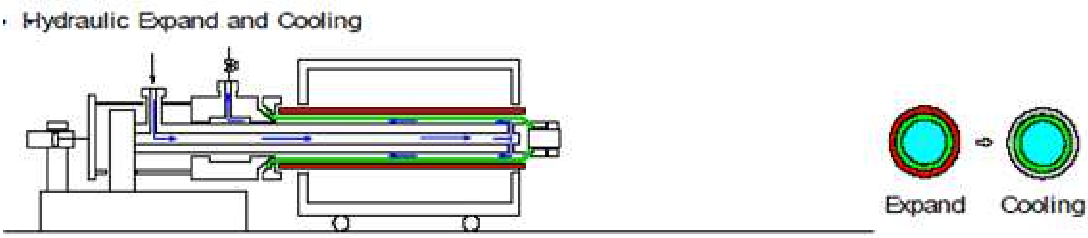

Figure Appendix A-4: Stage 3, Hydraulic expansion of the inner liner

Stage 4: Heating of the Liner Pipe

It is assumed that due to contact of the liner pipe with the heated outer pipe, the liner pipe heats up due to the temperature of the outer pipe. The liner pipe wants to expand but is not able to, because of the restriction of the outer pipe.

Stage 5: Relief of Internal Pressure

The hydraulic overpressure of the cooling water is removed, but the cooling water and oven are still active.

Stage 6: Relief of Temperature while Cooling the Inner Liner

At this stage of the manufacturing process, after the internal overpressure is removed in stage 5 from the process, the TFP is taken out of the oven and cooled down in the atmosphere. During this period, the liner pipe is still actively cooled by the cooling water. The active cooling of the liner pipe is assumed to continue until the outer pipe has reached T_{end} , which is 343 K (70°C). The cooling water is removed when this temperature in the outer pipe is reached, this will increase the temperature in the liner pipe up to 343 K.

Stage 7: Relief of Temperature without Cooling Water in the Inner Liner (Figure Appendix A-5)

The liner and the outer pipe cool down together from the temperature T_{end} to the room temperature T_{room}.

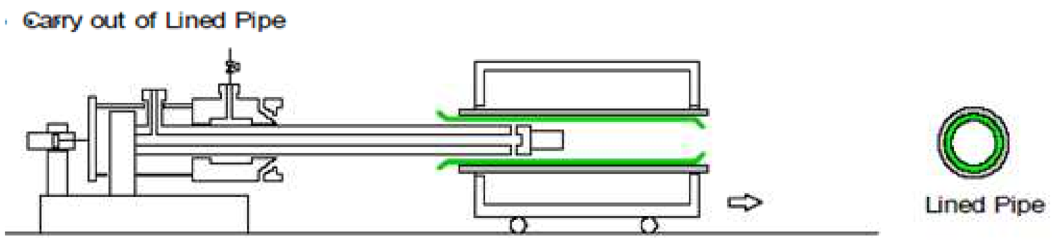

Figure Appendix A-5: Final stage, stage 7, cooling of the TFP in the atmosphere

-The effect of cooling on the residual hoop stress.

The amount of heating of the liner pipe has large influence on the residual stresses in the liner at the end of the manufacturing process. This is due to the fact that after heating up both pipes shrink due to cooling down. The amount of cooling depends on the temperature from which the cooling stage starts. The liner has a larger thermal expansion coefficient than the outer pipe. If the liner pipe is assumed to have a high temperature, from which the cooling starts, the liner will shrink significantly. If this is the case, the decrease in diameter of the liner will be larger than the decrease in diameter of the outer pipe; this will result in lower or even loss of gripping force. If the liner pipe is assumed to heat up only a small amount, the liner pipe will only shrink a small amount. The liner pipe will shrink less than the previous case, resulting in a larger gripping force. In order to determine the average temperature of the liner and the outer pipe, a numerical calculation is made, this is discussed in the following subsection.

Appendix B

Appendix B consists of the experimental set-up information

Experimental set-up consist of a force indicator (a), stationary compression pad (b) and test specimen with piston (c).

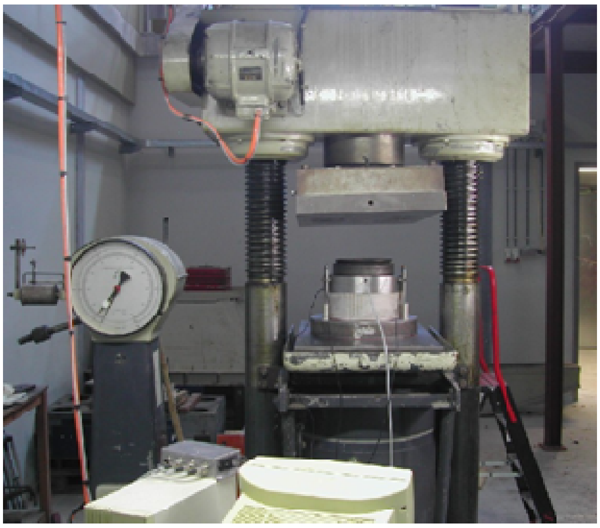

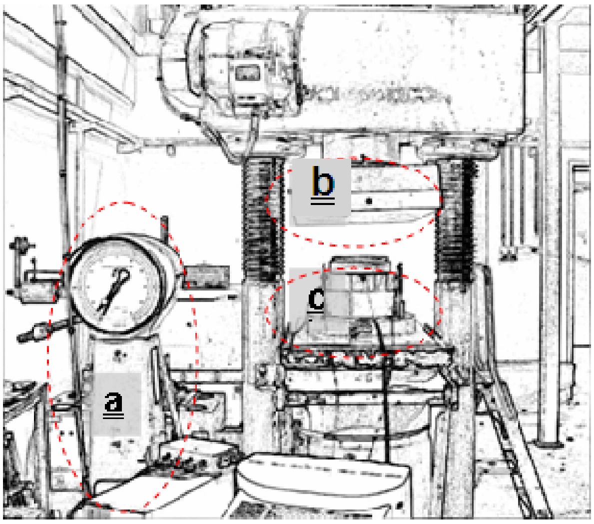

a, **b** and **c** are defined below

a: Force indicator with computer system for data collection

This force indicator is used to verify the hydraulic pressure gauge which is connected with the piston. The pressure gauge signal is recorded and stored on the computer.

The computer which is shown on the picture records the applied force, displacement of the piston (with the LVDT´s), strain (with the strain gauges) in the test specimen and duration of the recorded experiment.

Liner compression setup

b: Stationary compression pad with swivel.

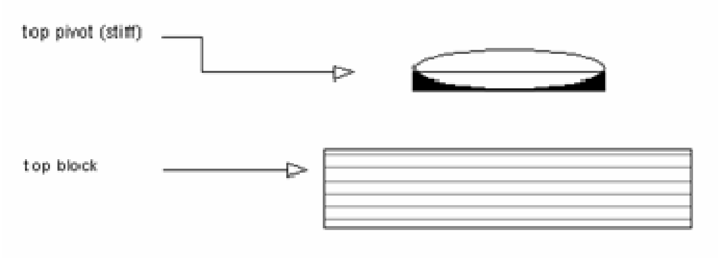

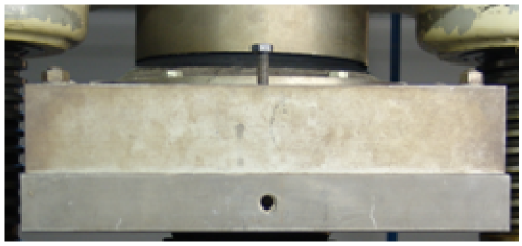

c: Experiment setup liner and TFP configuration

Liner configuration with piston driven compression block

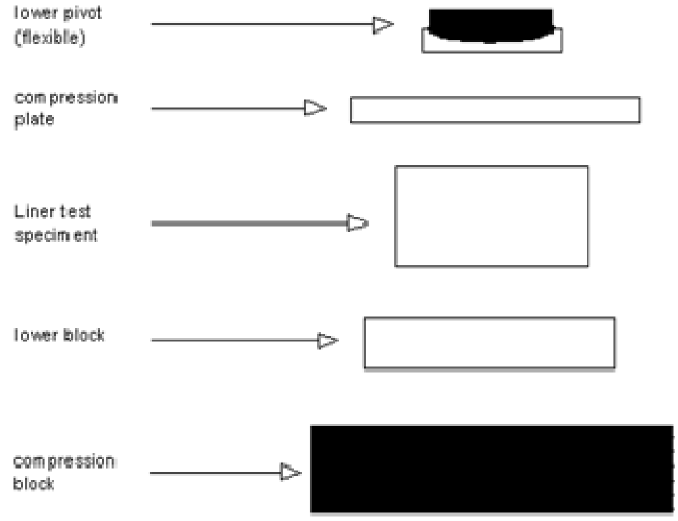

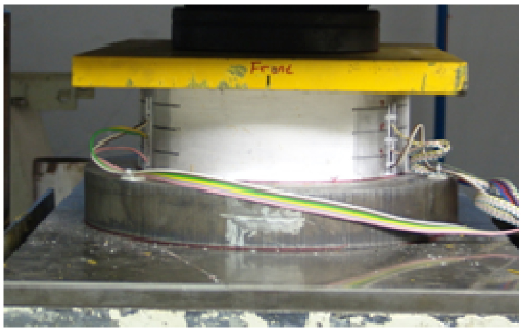

Compression plate for the liner (as seen in **c**):

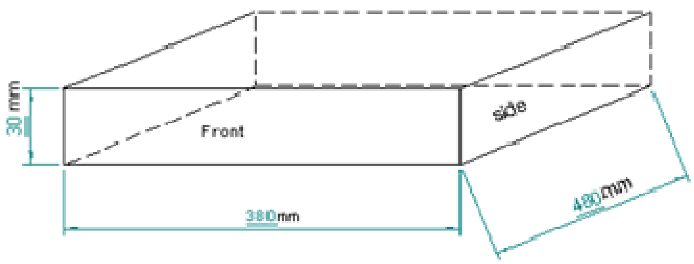

Appendix C

Appendix C is the Finite Element Method (FEM) section. This includes a description of the FEM process, the FEM Element type, FEM Meshing, FEM Boundary Conditions and Loading and Buckling Analysis

FEM Process

The process of making a FEM model starts with investigating the physical model. Idealization and discretization is then used to convert the physical model into a discrete model with a finite number of degrees of freedom within MSC.Marc 2005. This discrete model is then updated with experimental material properties so that it represents the physical model better, this is also called model updating and is used as a basis in this study, the physical model can be viewed in:

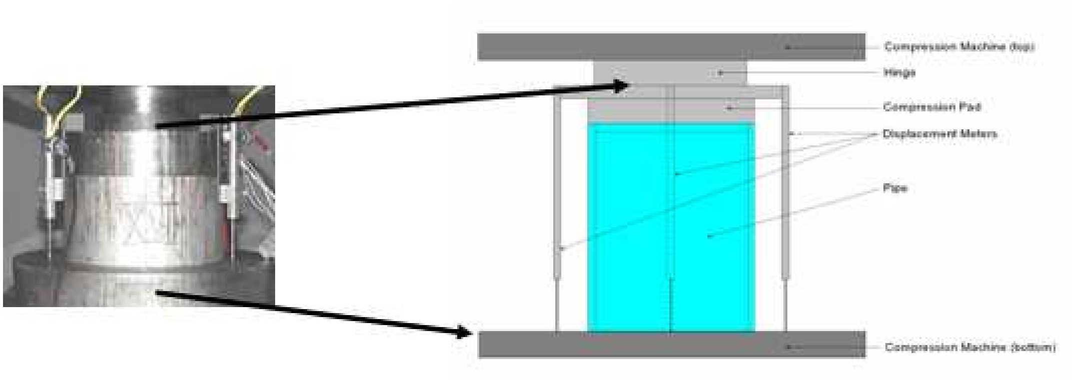

Figure Appendix C-1: Schematic Physical Model and Actual Model

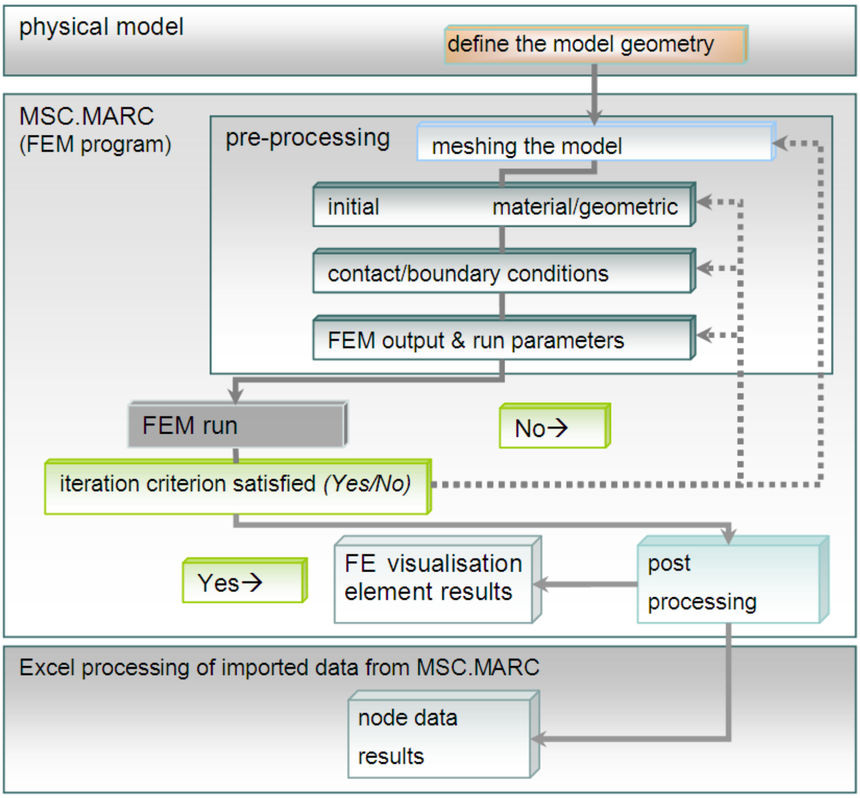

Figure Appendix C-2: Flowchart of the FEM

Element type

The element type is a very important feature for a FEM program. To some extent all finite element types are specialized and can only simulate a limited number of types of response. An important step in the finite element modelling procedure is choosing the appropriate element type, which should best suit to the simulation. The physics of the model should be understood well enough to make an appropriate choice of element type. It can give wrong results or even will not give any solutions when an element is chosen which is not applicable to the situation. Solid element types have been used, avoiding shell element. The schematic difference between the shell model and the solid model is illustrated by Figure Appendix C-3.

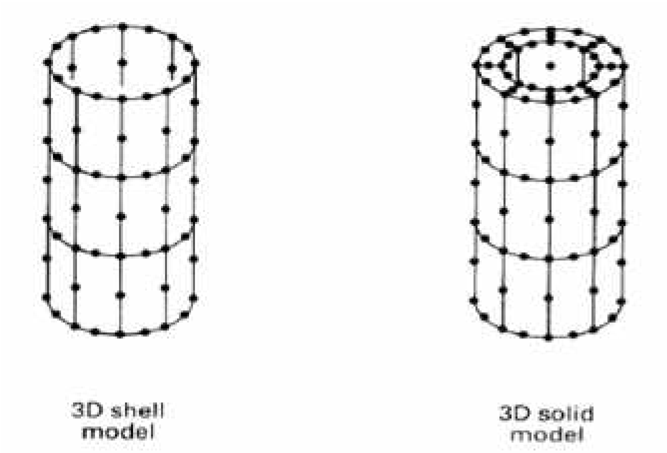

Figure Appendix C-3: 3D FEM Shell and Solid Cylinder

Shell elements ignore changes in thickness. Another advantage is that a solid element has more nodes to calculate the shape function of one element. A disadvantage is the computation cost compared to shell elements due to the larger number of nodes.

The elements of the cylinder are first made up in a 2D plane by use of 8-node quadrilateral elements. After which it is expanded into 3D hexahedron elements, see Figure Appendix C-4, which is also called “a 20-node quadratic” or “type 21” element in MSC.Marc.

Element type 21 is a full integration element. This element, with high computing costs, is preferred over type 57 which is a reduced integration element. These have less computing cost, but more are needed to simulate non-linear behaviour and do not yield significantly different results.

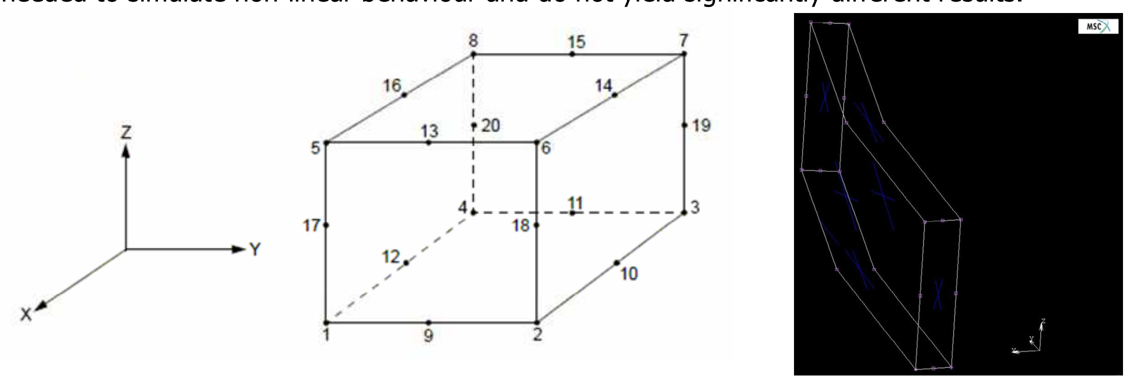

Figure Appendix C-4: Numbering of a Three-Dimensional 20–node solid FEM element

FEM Meshing

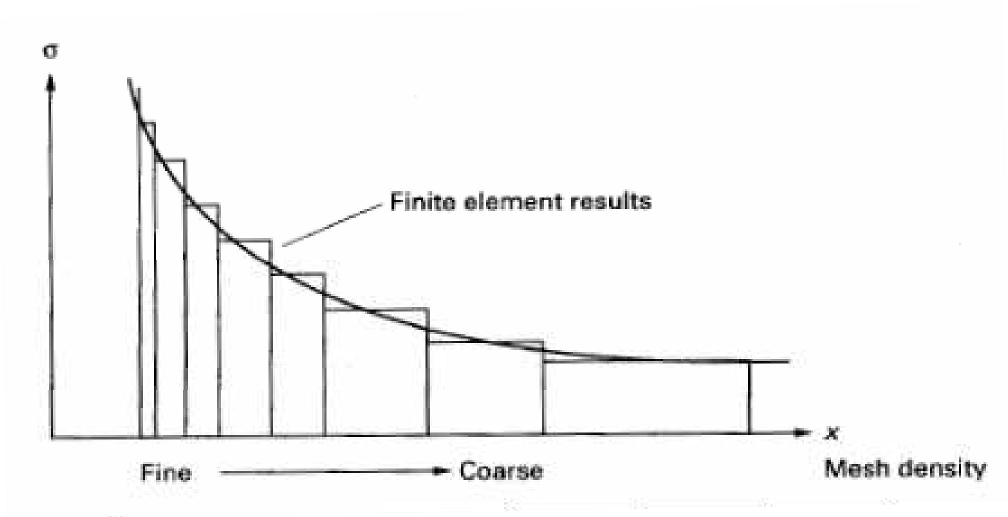

Figure Appendix C-5: Finite mesh density relationship vs. stress density

Mesh design or the discretization of a structure into a number of finite elements, is one of the most critical tasks in finite element modelling. The following parameters need to be considered carefully in designing the layout of elements: mesh density, and aspect ratio of the elements. A rectangular 1 by 1 element form is preferred over a skewed element or elongated one. As a general rule, a finer mesh is required in areas of high stress gradient, see Figure Appendix C-5. [Ref. 1]. Manual meshing of the number and form of the element mesh has been used in this study. The mesh density is a 20 element circumferential density and a 20 element longitudinal density. An increase in density does not yield significantly different results but a lower density will.

A full symmetrical model is made, this has been preferred over a fraction of the model. It is possible to simulate 90 degrees or less of the radius, but this was not of importance in this model. First the model is made up out of surface 2D elements, from this specified surface it is possible to convert a 2D cylinder ring into a 3D element cylinder, see Figure Appendix C-6.

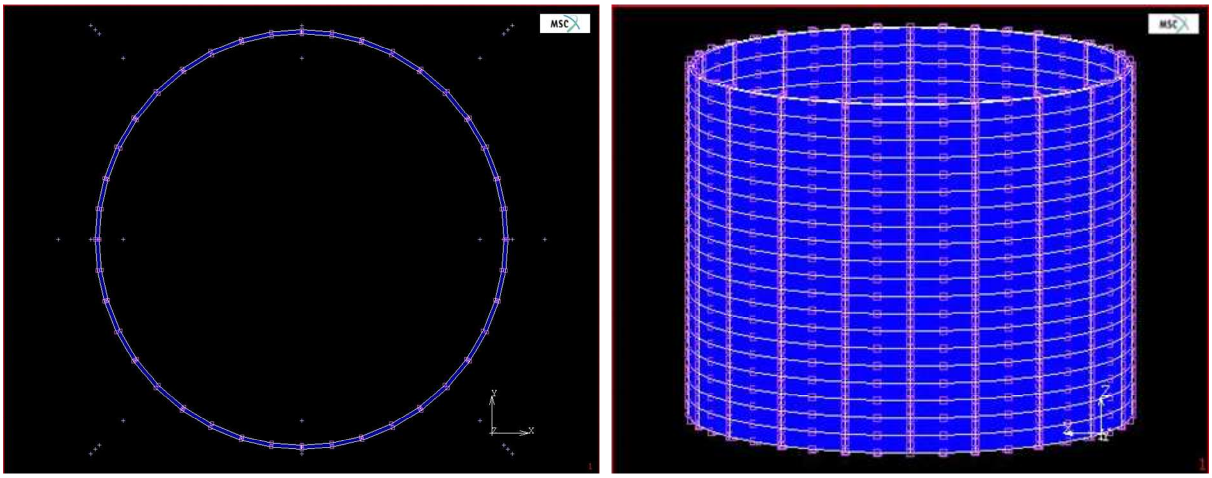

Figure Appendix C-6: 2D Cylinder ring and a 3D Cylinder build up out of elements

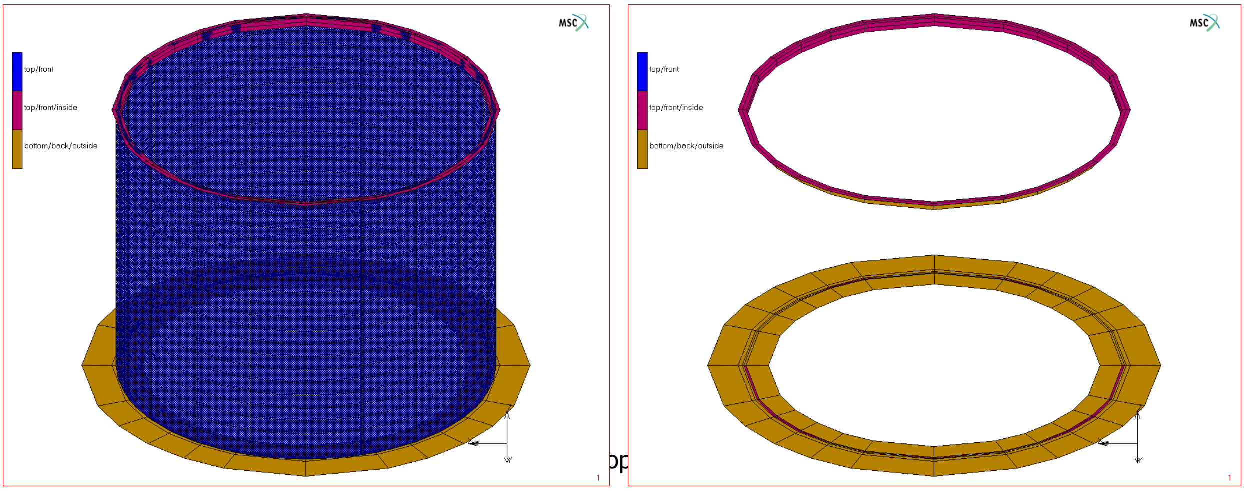

The next step is to make the base on which the cylinder "rests" and the piston/compression Pad which will move axially. The cylinder elements, the piston and base can be seen together in Figure Appendix C-7. These form the geometry of the FEM mesh. It is now possible to give all the segments properties, which will approach the physical properties of the physical model. First we will give the entities contact properties. It is possible to deform the cylinder with these bodies There are two main contact properties, deformable and rigid. Rigid bodies or un-deformable bodies, which can only consist of surfaces, are used to simulate the compression machine. The piston or compression pad will have a fixed displacement and the base will have no displacement. The cylinder will have a deformable property, which will be placed between the rigid bodies.

FEM Boundary Conditions

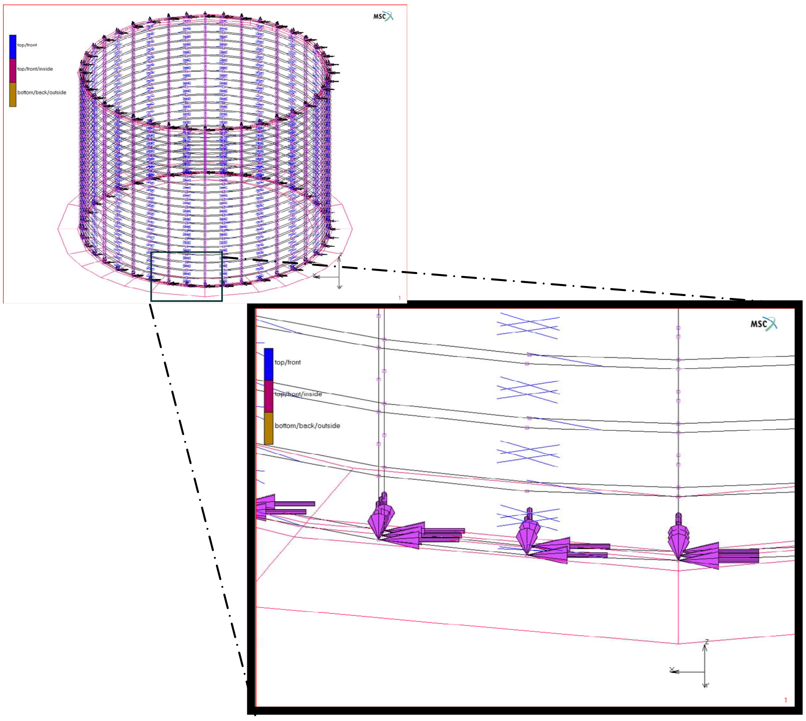

Figure Appendix C-8: Boundary Conditions at Nodes

An important task of the FEM model is in the selection of the FEM boundary conditions. Generally, the support condition is idealized as completely rigid or completely free. In reality the support condition is usually somewhere in between. The most popular technique used to minimize the impact on the analysis of the assumptions made in boundary conditions is to develop a model large enough such that the area of interest is sufficiently remote from the boundary. [Ref. 1].
The boundary conditions, (BC), are taken at end nodes of the elements bordering the cylinder ends where the rigid bodies contact the cylinder, see Figure Appendix C-8. The BC will be set at zero displacement in the X and Y plane or u and v direction, also called clamped BC's. This will simulate infinite friction during the axial compression in the contact area, which is applicable assuming the practical experiments of Focke [Ref. 12].

Loading and Buckling Analysis

Nodal displacement is used in this study, which will convert nodal displacement into nodal reaction forces. The nodes react to this displacement and give information on the forces and strains during this action. A displacement of 1 mm and 2 mm was used for the 100mm and 200mm liner to simulate a strain of 1 percent.

Two techniques are available for performing a FEM buckling analyses, non-linear buckling analysis and eigenvalue buckling analysis.

Non-linear buckling analysis is usually the more accurate approach. This technique employs a non-linear static analysis with gradually increasing loads/displacements to seek the load level at which a structure becomes unstable. But the disadvantage is that it needs additional information when used on some geometries, for example on a cylinder. The FEM program MSC.Marc does not support buckling of a perfect pipe in perfect conditions. If the geometry will be axially compressed without a buckling mode, buckling will then initiate only when a numerical round-off-error arises.

The second method, eigenvalue buckling analysis, predicts the theoretical buckling strength of an ideal linear elastic structure. This method corresponds to the textbook approach to elastic buckling analysis: for instance, an eigenvalue buckling analysis of a column will match the classical Euler solution. However, imperfections and non-linearities prevent most real-world structures from achieving their theoretical elastic buckling strength.

In all models, prior to the eigenvalue solution, a pre-stressed structure was created with a unit pressure load. This pre-stressed structure was submitted to the eigenvalue loadcase to determine the modeshape. Since the eigenvalues are simply the load multipliers, and the pre-stressed structure had a unit load, the lowest eigenvalue would correspond to the theoretical buckling mode.

The information from the eigenvalue solution was used as a reference point for the non-linear analysis. In the nonlinear run, ramped pressure loading was applied on the structure until buckling occurs. The pressure load was also normalized with respect to the time substeps, i.e. the pressure load and the corresponding time substep are equal in magnitude, for convenience in postprocessing. An initial perturbation force was applied at certain points to induce instability. Obviously, the resulting computed critical pressure varied with the applied perturbation force. In the actual structure, this perturbation force may represent an initial structural imperfection. Hence, prior to a nonlinear run, a quick linear-elastic static run was performed to determine the radial deformation of the cylinder caused by the perturbation force without any pressure load. One then may argue that this deformation could represent the initial "out-of-roundness" that would trigger elastic instability. This may not be a totally valid argument, but at the very least, I ran a few cases that showed the relative change in critical pressure with respect to a change in the applied trigger force.

*The option in MSC.Marc to perform a perturbation of the geometry by the buckling mode is not yet supported by MSC.Marc 2005 and must be entered into the input file by the user.

Appendix D

Axial compression of the liner TFP configuration.

The setup is identical as the liner setup in Appendix B, but with a different Compression plate, applicable on the TFP pipe, with displacement indicators.

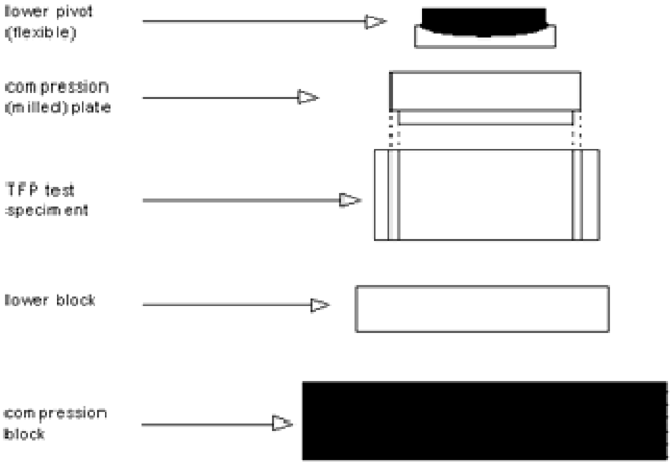

LVDT's are Linear variable displacement transducers. These transducers registers the axial displacement of the liner compression (milled) plate.

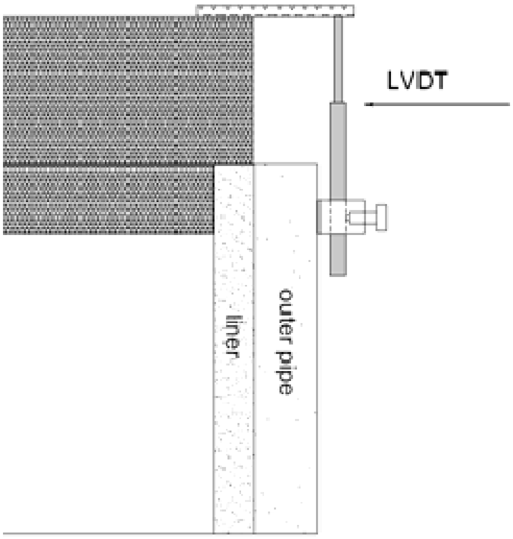

Schematic representation (left) and picture (right) of the LVDT setup

Appendix E

3D PLUTO data processed in MATLAB of TFP Orange 1, Green

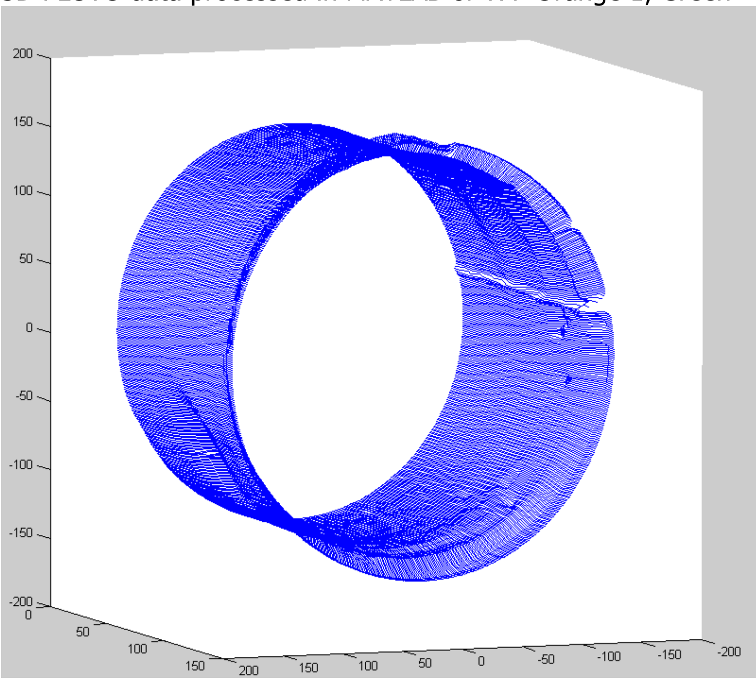

Figure Appendix E-1: TFP 3D Image of Orange 1

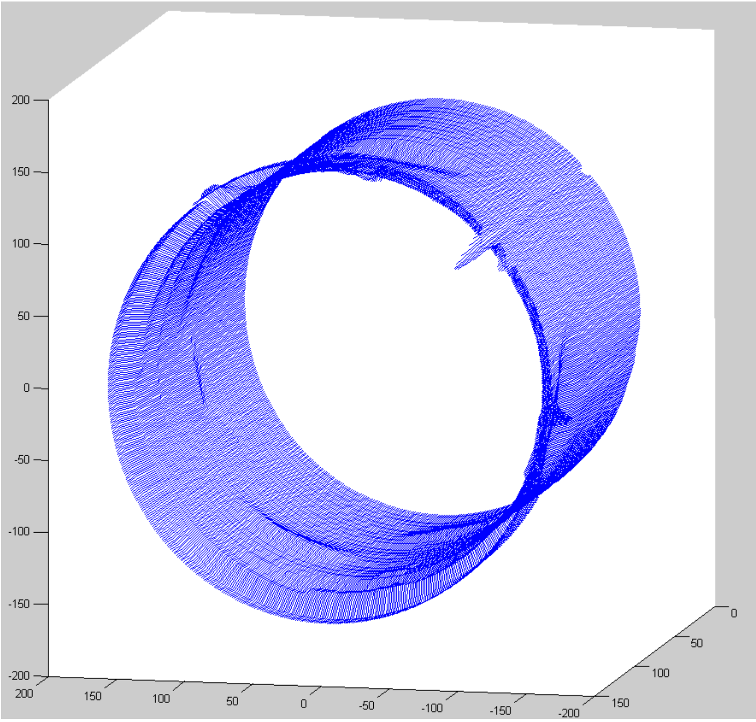

Figure Appendix E-2: TFP 3D Image of Green 6

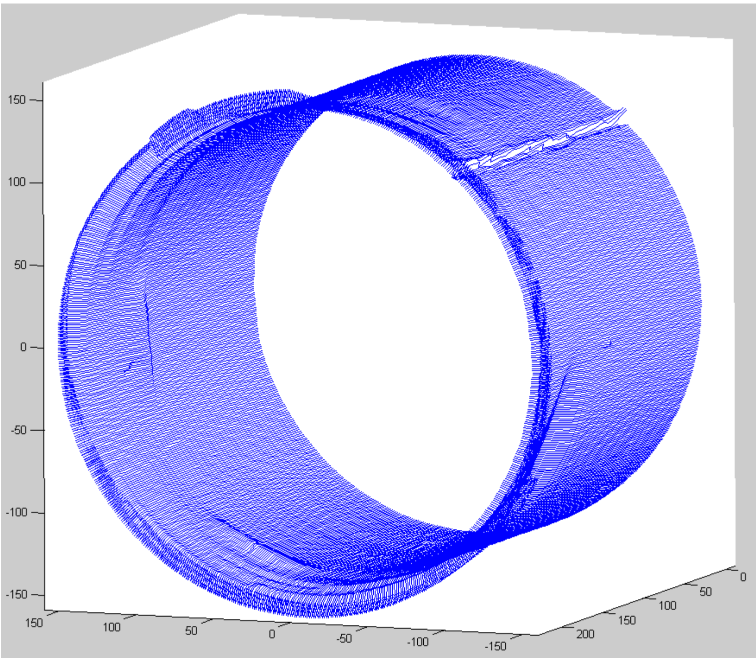

Figure Appendix E-3: TFP 3D Image of Orange 6

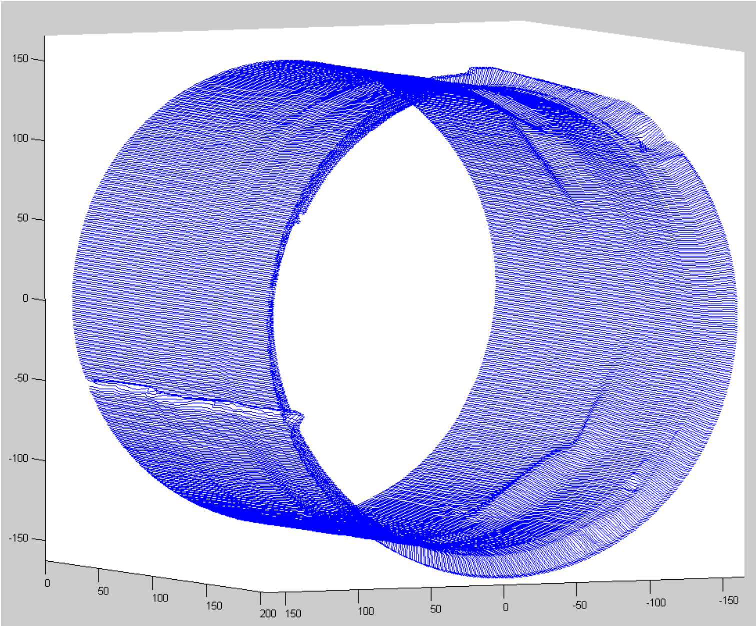

Figure Appendix E-4: TFP 3D Image of White 3

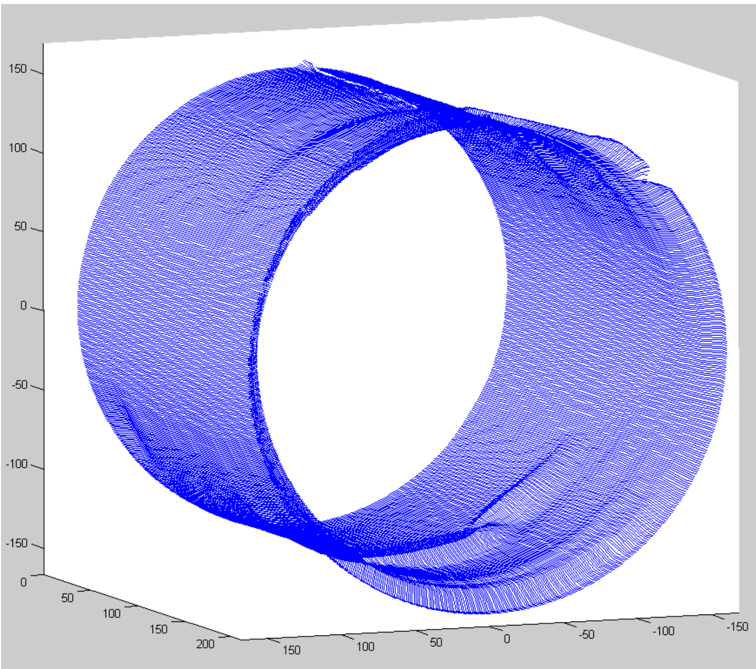

Figure Appendix E-5: TFP 3D Image of White 4

List of Tables

List of Figures

List of Equations